Power Engineering and Engineering Thermophysics
https://www.acadlore.com/journals/PEET

Analysis of Fluid Velocity and Static Pressure Dynamics in a Convergent-Divergent Nozzle: Integration of Soft Computing Techniques with CFD

Nindia Nova Novena[1], Zainal Arifin[2], Catur Harsito[3,4], Abram Anggit Mahadi[5], Mochamad Subchan Mauludin[6], Rafiel Carino Syahroni[7], Yuki Trisnoaji[1], Singgih Dwi Prasetyo[1*]

[1] Department of Power Plant Engineering Technology, Faculty of Vocational Studies, State University of Malang, 65145 Malang, Indonesia
[2] Department of Mechanical Engineering, Faculty of Engineering, Universitas Sebelas Maret, 57126 Surakarta, Indonesia
[3] Department of Mechanical Engineering, Faculty of Vocational, Universitas Sebelas Maret, 57126 Surakarta, Indonesia
[4] Department of Mechanical Computer Industrial and Management Engineering, Kangwoon National University, 25913 Samcheok, Korea
[5] Department of Mechanical Systems and Engineering, Gifu University, 501-1193 Gifu, Japan
[6] Department of Informatics Engineering, Faculty of Engineering, Universitas Wahid Hasyim, 50236 Semarang, Indonesia
[7] Department of Mechanical Engineering, Cheng Shiu University, 83347 Kaohsiung City, Taiwan

[*] Correspondence: Singgih Dwi Prasetyo (singgih.prasetyo.fv@um.ac.id)

Received: 11-16-2024 **Revised:** 12-15-2024 **Accepted:** 12-23-2024

Citation: N. N. Novena, Z. Arifin, C. Harsito, A. A. Mahadi, M. S. Mauludin, R. C. Syahroni, Y. Trisnoaji, and S. D. Prasetyo, "Analysis of fluid velocity and static pressure dynamics in a convergent-divergent nozzle: Integration of soft computing techniques with CFD," *Power Eng. Eng. Thermophys.*, vol. 3, no. 4, pp. 209–243, 2024. https://doi.org/10.56578/peet030401.

Abstract: A novel approach for analyzing fluid flow dynamics and static pressure distributions within a convergent-divergent nozzle was presented, integrating soft computing techniques with computational fluid dynamics (CFD) simulations performed using Ansys Fluent. The study differs from traditional CFD approaches by leveraging soft computing methods to optimize simulation parameters and enhance the accuracy of predictions. Four distinct fluids—air, hydrogen, nitrogen, and helium—were analyzed across a range of inlet velocities (1 m/s to 5 m/s). The study systematically evaluates the influence of boundary conditions and flow models, including both viscous and inviscid conditions, on the flow patterns and static pressure distributions. The results highlight the substantial impact of fluid density and viscosity on the flow dynamics, particularly for lighter gases such as hydrogen and helium. These gases exhibit higher velocities and less pronounced pressure gradients due to their lower density and viscosity compared to denser fluids like air and nitrogen. Soft computing techniques improve the reliability of these findings by enhancing the predictive capability of the CFD model, allowing for more precise insights into complex fluid behaviors. The implications of these findings are significant across multiple engineering domains, such as aerospace propulsion, chemical processing, and energy systems, where optimizing fluid flow characteristics is critical. The integration of soft computing with CFD provides a robust framework for more accurate modelling of low-density, high-velocity flows and offers valuable insights for the design of more efficient systems. This study underscores the potential of advanced computational techniques in advancing both fluid dynamics research and engineering applications.

Keywords: Fluid mechanics; Soft computing; Nozzle; Static pressure; Velocity magnitude

1 Introduction

1.1 Background

In modern industry and technology, optimizing nozzle design plays a crucial role in various applications, including rocket propulsion systems, gas turbines, and fluid injection systems [1]. The fluid flow characteristics within a nozzle

is a critical factor influencing the performance efficiency of these devices [2]. One of the most widely used approaches for studying nozzle flow behavior is CFD. Through simulation tools such as Ansys Fluent, researchers can analyze flow parameters, including static pressure and velocity magnitude, to predict and optimize nozzle performance [3, 4].

Fluid flow dynamics in nozzles are significantly influenced by the physical and thermodynamic properties of the fluid, such as density, viscosity, and specific heat capacity [5]. These properties determine the interaction between the fluid and the nozzle walls, impacting key performance metrics such as thrust, flow uniformity, and energy transfer efficiency. This relationship highlights the need to explore the effects of fluid characteristics on nozzle performance to guide design optimization in industrial applications.

This study focuses on comparing viscous and inviscid fluid flows within a nozzle. The research aims to provide a comprehensive understanding of how fluid viscosity influences the distribution of static pressure and velocity magnitude at the nozzle outlet. The choice to analyze viscous and inviscid flows stems from their fundamental differences in fluid dynamics [6]. Inviscid flow, an idealized concept that assumes no viscosity, represents flow without frictional effects, while viscous flow accounts for the effects of viscosity, resulting in significant alterations in flow profiles [7, 8]. A key objective of this research is to investigate how soft computing techniques can improve the analysis of fluid properties in nozzle designs. Unlike conventional CFD approaches, integrating soft computing methods provides new opportunities to optimize simulation parameters and enhance predictive accuracy, especially in scenarios involving complex fluid behaviors [9, 10].

The fluid parameters considered in this study include three types of fluids: air, hydrogen, and helium. These fluids were selected based on their unique thermodynamic and transport properties, significantly influencing flow distribution within the nozzle. Each fluid was analyzed at five inlet velocity levels (1, 2, 3, 4, and 5 m/s) to explore the relationship between inlet velocity and the distribution of pressure and velocity throughout the nozzle [11, 12]. This research is essential because static pressure and velocity magnitude are key parameters in nozzle design [13]. Static pressure contributes to the nozzle's ability to generate thrust or regulate mass flow rate, while the outlet velocity determines the overall efficiency of the system [14, 15]. A comparative analysis involving various fluid parameters provides insights into how viscosity and thermodynamic properties influence nozzle performance [16, 17].

Using CFD simulation via Ansys Fluent, this study offers quantitative data and comprehensive visualization of flow dynamics within the nozzle [18]. This approach provides high flexibility in modeling complex flows, enabling researchers to gain a detailed understanding of flow mechanisms. Furthermore, such simulations can validate theoretical predictions and laboratory experiments, enhancing the reliability of the research outcomes [12, 19–23]. CFD methods have been widely employed in prior studies to investigate flow phenomena within nozzles [4]. For instance, it has been demonstrated that pressure and velocity distributions in a nozzle are significantly influenced by fluid viscosity, especially in flows with low Reynolds numbers. Additionally, it can be observed that low-viscosity fluids like helium tend to produce higher outlet velocities than higher-viscosity fluids such as air or nitrogen [22]. The findings of this research have significant industrial implications. For example, in aerospace propulsion systems, optimizing nozzle design for low-density and high-velocity flows can enhance thrust efficiency. Similarly, in chemical processing and energy systems, understanding the influence of fluid viscosity on flow dynamics aids in designing more efficient mass transfer and heat exchange processes [23].

The effect of fluid type on flow characteristics has also been extensively studied [3]. It has been highlighted those thermodynamic properties, such as density and specific heat capacity, impact flow patterns and pressure distribution within nozzles [24]. For example, helium, with its low density and high thermal conductivity, exhibits distinct flow patterns compared to nitrogen or air [9, 25]. This research aims to fill gaps in the existing literature by providing a thorough comparison between viscous and inviscid flows across four fluid types at various inlet velocities [26]. The analysis is expected to contribute significantly to the understanding of fluid flow dynamics in nozzles and its implications for industrial device design [3, 27]. Thus, the findings of this study may serve as a reference for developing fluid flow systems across diverse sectors [6, 28].

1.2 State of the Art

Table 1 highlights recent research efforts using CFD to study the flow of air, helium, and hydrogen under multiple regimes. While these studies primarily rely on traditional CFD approaches, they present significant opportunities for integrating soft computing and data mining techniques to enhance the depth and scope of the analysis. Soft computing methods, such as artificial neural networks (ANNs) and fuzzy logic, can improve the predictive capabilities of CFD models by addressing uncertainties and non-linear relationships that traditional methods may overlook. For instance, in the study on hydrogen production using oxygen transport membranes, ANN models could complement the Wagner equation to predict variations in oxygen flux under diverse conditions.

Similarly, data mining techniques enable efficient feature extraction and pattern recognition from large simulation datasets. These methods can identify critical parameters, such as velocity or pressure distributions, significantly impacting flow behavior. For example, the validation of hydrogen safety simulations in one study could benefit from clustering algorithms to automate the classification of safe and unsafe scenarios. Regression or support vector

machine (SVM) models could also predict leakage scenarios in hydrogen-blended natural gas systems, providing valuable insights for safety enhancements.

Table 1. State of the art

Journal Name	Publication Year	Paper Title	Motion Model Used	Feature Extraction and Observation Model Used	Reference
Membranes	2023	CFD Modelling of Hydrogen Production via Water Splitting Using Oxygen Transport Membranes	Stationary laminar flow model	Feature extraction using Wagner's equation for oxygen flux; observation model using partial oxygen pressure chemical equilibrium	[29]
Energies	2023	Validation and Verification of Containment Foam CFD Simulations in Hydrogen Safety Analysis	Turbulent flow model with OpenFOAM	Feature extraction through validation against experimental data; observation model using hydrogen safety analysis	[30]
ACS Omega	2023	Numerical Simulation Analysis of the Hydrogen-Blended Natural Gas Leakage in Domestic Kitchens	Turbulent flow model with CFD	Feature extraction through hydrogen-natural gas mixture analysis; observation model using leakage simulation in domestic kitchens	[31]

Soft computing techniques also support optimizing simulation parameters, such as turbulence models or boundary conditions, through genetic algorithms or particle swarm optimization (PSO). This capability ensures more accurate and computationally efficient CFD results. Moreover, fuzzy inference systems or clustering can enhance observation models by incorporating adaptability to diverse conditions, such as those encountered in hydrogen safety or production scenarios. These methodologies showcase the potential of soft computing and data mining to streamline CFD analysis and open new avenues for uncovering complex flow patterns and behaviors.

2 Methodology

In Figure 1, the flowchart illustrates the steps taken during the simulation using Ansys Fluent software. The process begins with opening Ansys Fluent and setting up the boundary conditions, selecting the fluid type (air, hydrogen, nitrogen, helium) and inlet velocity (1 m/s, 2 m/s, 3 m/s, 4 m/s, and 5 m/s). The inlet velocity range (1 m/s to 5 m/s) was chosen to simulate conditions that represent a gradual increase in flow dynamics, which is critical for understanding transitions in flow regimes from laminar to turbulent. Those fluids were chosen due to their distinct thermodynamic and transport properties, such as density, viscosity, and thermal conductivity, which significantly influence flow behavior within the nozzle. Once the boundary conditions were established, two main approaches were used for the simulation: the viscous model, which accounts for the fluid's viscosity effects, and the inviscid model, which assumes an ideal scenario without viscosity effects. The results from both approaches were then analyzed using Analysis of Variance (ANOVA) to evaluate differences and determine the outcomes. This study integrates soft computing techniques, specifically ANNs, to enhance the analysis of flow patterns and optimize simulation parameters. The ANN model was structured with multiple hidden layers to capture non-linear relationships in the flow data, improving the accuracy of predictions compared to conventional CFD approaches. Additionally, fuzzy logic was implemented to address uncertainties in boundary conditions, enabling more adaptive and robust simulation outcomes. This diagram provides a systematic step-by-step guide for conducting fluid dynamics simulations with Ansys Fluent, which is crucial for ensuring the validity and accuracy of the simulation results. Figure 2 shows the boundary conditions of this study. The boundary conditions for the simulation included a fixed inlet velocity for each case, a pressure outlet set to atmospheric pressure (1 atm) to allow natural flow exit, and no-slip wall conditions along the nozzle's surface to account for viscous effects. These conditions ensure realistic modeling of the interaction between the fluid and the nozzle walls while maintaining consistency across all simulations.

3 Equations

Below present key equations relevant to fluid mechanics, particularly for analyzing static pressure, velocity, and flow characteristics of air, hydrogen, helium, and Reynolds number (Re). Each equation is accompanied by its reference for further reading. Table 2 shows the parameters of the model.

Bernoulli's equation is as follows:

$$P = \text{Constant} \frac{1}{2}\rho V^2 \tag{1}$$

where, P is the static pressure (Pa), ρ is the air density $\left(\mathrm{kg/m^3}\right)$, and v is the fluid velocity $(\mathrm{m/s})$.

This fundamental equation in fluid mechanics relates pressure and velocity in inviscid, steady flows. It is instrumental in determining the static pressure of air [32].

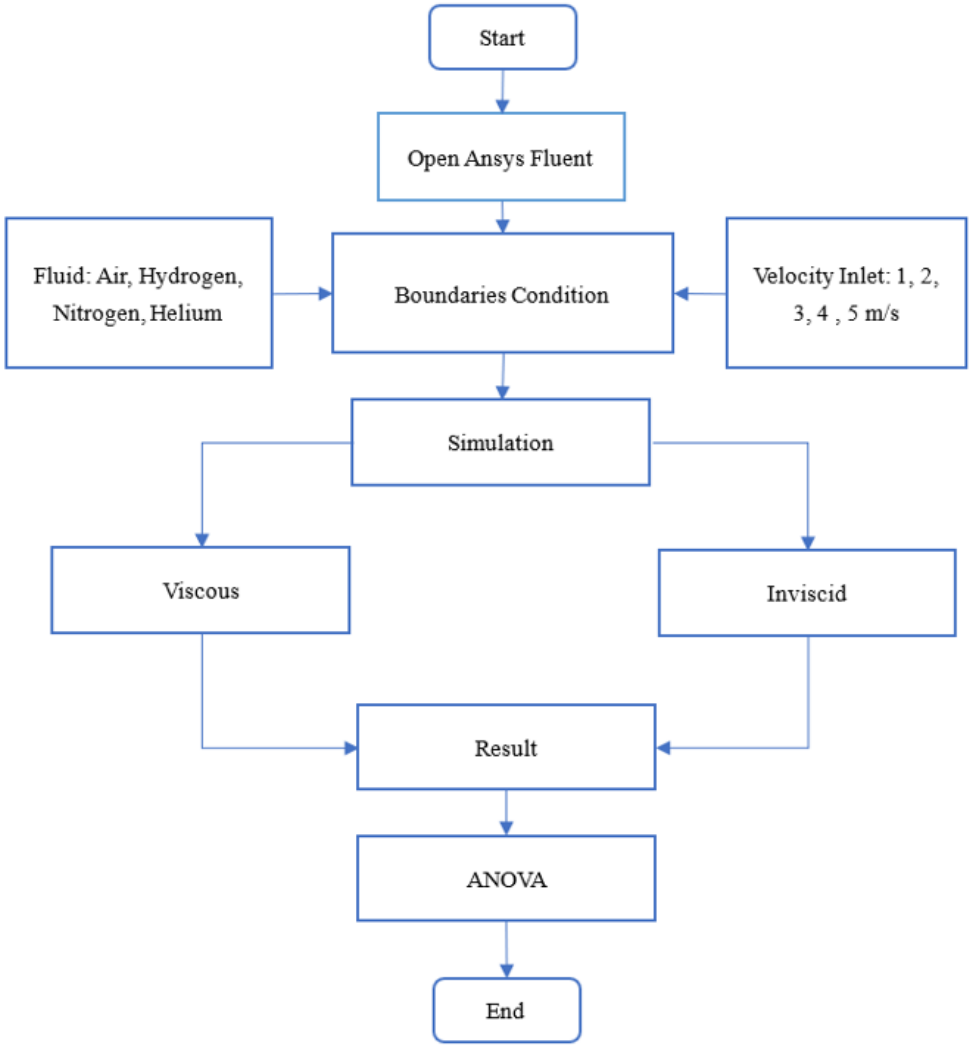

Figure 1. Flowchart

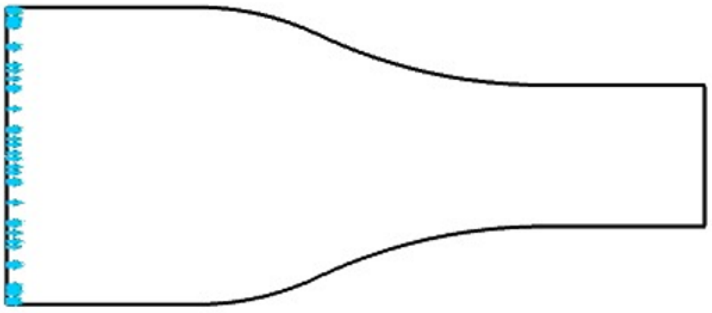

Figure 2. Boundary conditions

Table 2. Key parameters of the proposed model

Fluid	Density ($\mathrm{kg/m^3}$)	Viscosity (Pa.s)	Kinematic Viscosity ($\mathrm{m^2/s}$)
Air	1225	1.81×10^{-5}	1.48×10^{-5}
Hydrogen	0.0899	8.76×10^{-6}	9.75×10^{-5}
Helium	0.1785	1.96×10^{-5}	1.10×10^{-5}

The continuity equation is as follows:

$$A_1 v_1 = A_2 v_2 \tag{2}$$

where, $A_1 v_1$ is the cross-sectional area of the channel at two different points $\left(\mathrm{m}^2\right)$, and $A_2 v_2$ is the flow velocity at two different points ($\mathrm{m/s}$).

This equation expresses the conservation of mass in incompressible fluid flow, indicating that the product of cross-sectional area and velocity remains constant along a streamline [33].

The velocity from pressure difference is expressed as follows:

$$\frac{v = \sqrt{2\left(P_1 - P_2\right)}}{\rho} \tag{3}$$

where, P_1 is the pressure at the first point (Pa), P_2 is the pressure at the second point (Pa), and ρ is the density of air in that condition $\left(\mathrm{kg/m^3}\right)$. This formula is used to find the velocity magnitude. A fluid's velocity can be calculated based on the pressure difference between two points, derived from Bernoulli's principle [34].

The ideal gas law for hydrogen is expressed as follows:

$$P = \rho R T \tag{4}$$

where, ρ is the hydrogen density $\left(\mathrm{kg/m^3}\right)$, R is the specific gas constant for hydrogen (about 4124 J/(kg-K)), and T is the temperature in Kelvin (K). This formula is used to find the static pressure for the hydrogen fluid. It relates the pressure, density, and temperature of hydrogen gas, which is essential for determining static pressure in varying conditions [35].

The average molecular velocity is expressed as follows:

$$\frac{\mathrm{vavg} = \sqrt{3 k_B T}}{m} \tag{5}$$

where, k_B is the Boltzmann constant (1.38×10-23J/K1.38×10 -23J/K), T is the temperature in Kelvin (K), and m is the molar mass of hydrogen molecule $\left(\sim 2 \times 10^{-3}\ \mathrm{kg/mol} \sim 2 \times 10^{-3}\ \mathrm{kg/mol}\right.$ divided by Avogadro's number). This equation determines the average velocity of gas molecules, pertinent in kinetic theory and gas dynamics [36].

The hydrostatic pressure equation is as follows:

$$P = P_0 + \rho g h \tag{6}$$

where, P is the static pressure at depth h(Pa), P_0 is the atmospheric pressure or initial pressure at the surface (Pa), ρ is the helium density $(\mathrm{kg/m^3})$, g is the acceleration of gravity $\left(\mathrm{m/s^2}\right)$, and h is the depth or height from the surface to the measured point (m).

Note: The density of helium can vary depending on temperature and pressure conditions. At room temperature and atmospheric pressure, the density of helium is roughly about 0.1785 $\mathrm{kg/m^3}$. The pressure at a certain depth in a fluid can be calculated, accounting for atmospheric pressure and the weight of the fluid column [37].

The dynamic pressure velocity relation is expressed as follows:

$$\frac{v = \sqrt{2 P_d}}{\rho} \tag{7}$$

where, P_d is the dynamic pressure (Pa), and ρ is the helium density $\left(\mathrm{kg/m^3}\right)$. Fluid velocity can be derived from dynamic pressure measurements, which is helpful in various aerodynamic calculations [37].

The Navier-Stokes equation is as follows:

$$\frac{\partial \vec{v}}{\partial t} + (\vec{v} \cdot \nabla)\vec{v} = -\frac{1}{\rho}\nabla P + \vec{g} \tag{8}$$

where, $\vec{v}$ is the fluid velocity (m/s), ρ is the fluid density $\left(\mathrm{kg/m^3}\right)$, P is the fluid pressure (Pa), and $\vec{g}$ is the acceleration of gravity $\left(\mathrm{m/s^2}\right)$.

For low velocities (1-5 m/s), the assumptions of steady flow (constant time) and incompressible flow (constant density) allow simplification. Thus, only pressure and acceleration affect the fluid. The fundamental equation describes the motion of viscous fluid substances, accounting for velocity, pressure, density, and external forces [38].

When $Re < 2000$, it means laminar flow; when $Re > 4000$, it means turbulent flow; when $2000 \leq Re \leq 4000$, it means transition.

The formula of the Reynolds number is as follows:

$$Re = \frac{v}{\mu} = \frac{vL}{v} \tag{9}$$

where, L is the characteristic length (m), μ is the dynamic viscosity $\left(\mathrm{kg.m^{-1}\,s^{-1}}\right)$, and v is the acceleration of gravity $\left(\mathrm{m/s^2}\right)$. Re is a dimensionless parameter to predict flow regimes. For air, helium, and hydrogen, respectively, it is calculated as follows [38]:

$$Re = \frac{v}{1.48 \times 10^{-5}}$$
$$Re = \frac{v}{1.10 \times 10^{-4}}$$
$$Re = \frac{v}{9.75 \times 10^{-5}}$$

4 Results

4.1 Viscous

4.1.1 Pressure of air

Figure 3 shows the static pressure distribution in a converging-diverging nozzle at different air velocities, namely 1 m/s, 2 m/s, 3 m/s, 4 m/s, and 5 m/s. Red indicates higher pressure, while blue indicates lower pressure. The pressure values range from 1.00 Pa to 16.12 Pa. At the inlet of the nozzle, the initial pressure is relatively high at lower speeds (1 m/s to 2 m/s), indicated by red to orange colors. The initial pressure remains high at higher speeds (3 m/s to 5 m/s), but the pressure drop is more significant as the fluid passes through the converging section. The pressure decreases for all speeds in the converging section, as seen from the color shift from red to green and blue. This drop is more pronounced at higher speeds, indicating more excellent fluid acceleration. At a speed of 5 m/s, the pressure drop in the converging section is very drastic, with the blue area dominating, indicating significant acceleration. The pressure increases again in the diverging section for all speeds, changing the color from blue to green and yellow. This pressure increase is more noticeable at lower speeds compared to higher speeds.

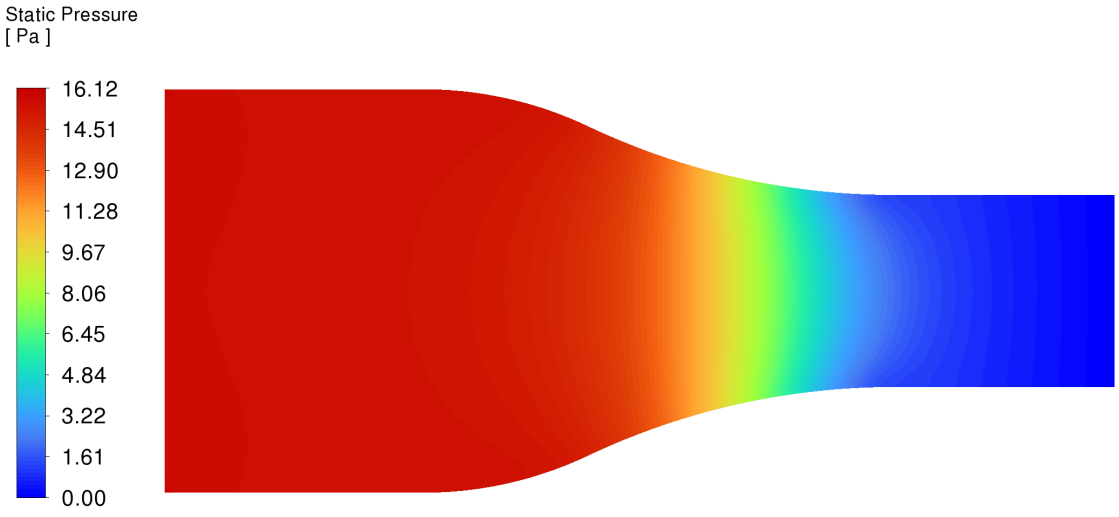

(a) Pressure of air at 1 m/s

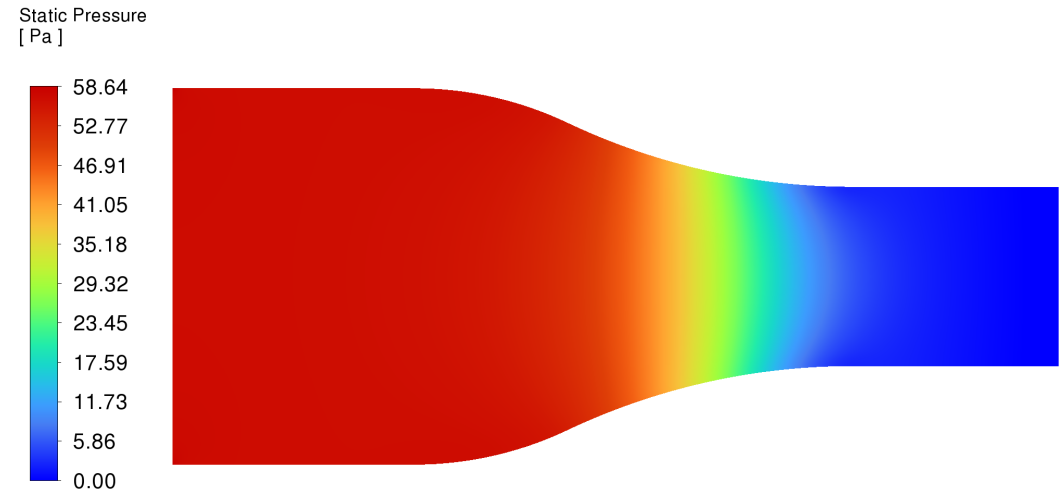

(b) Pressure of air at 2 m/s

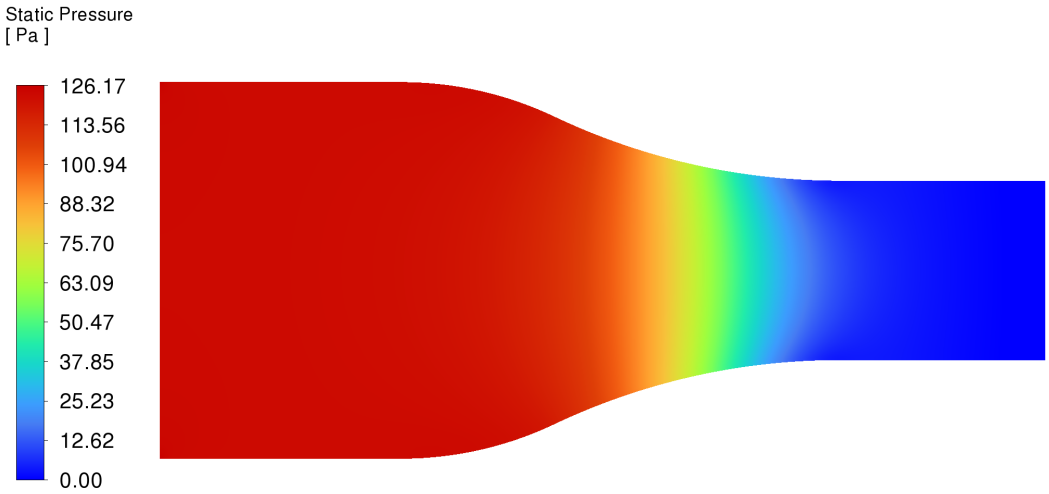

(c) Pressure of air at 3 m/s

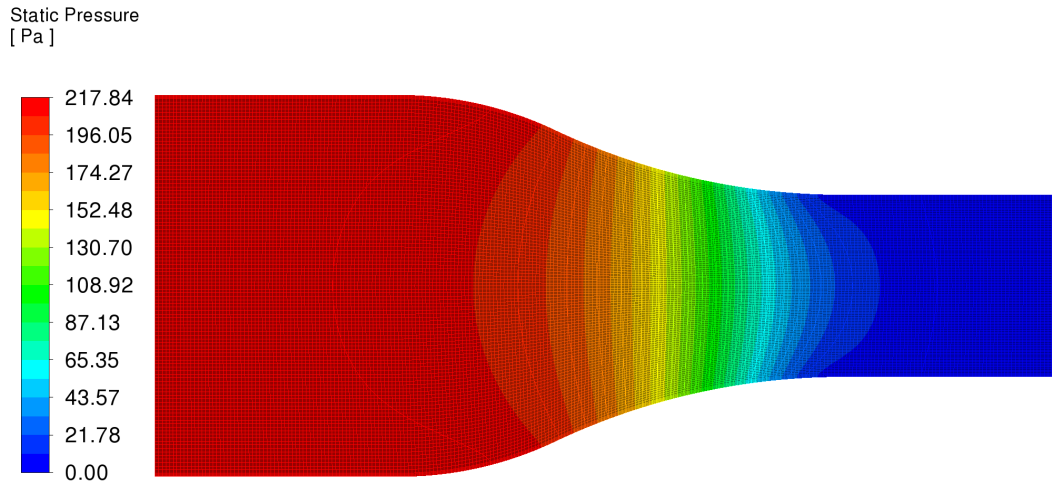

(d) Pressure of air at 4 m/s

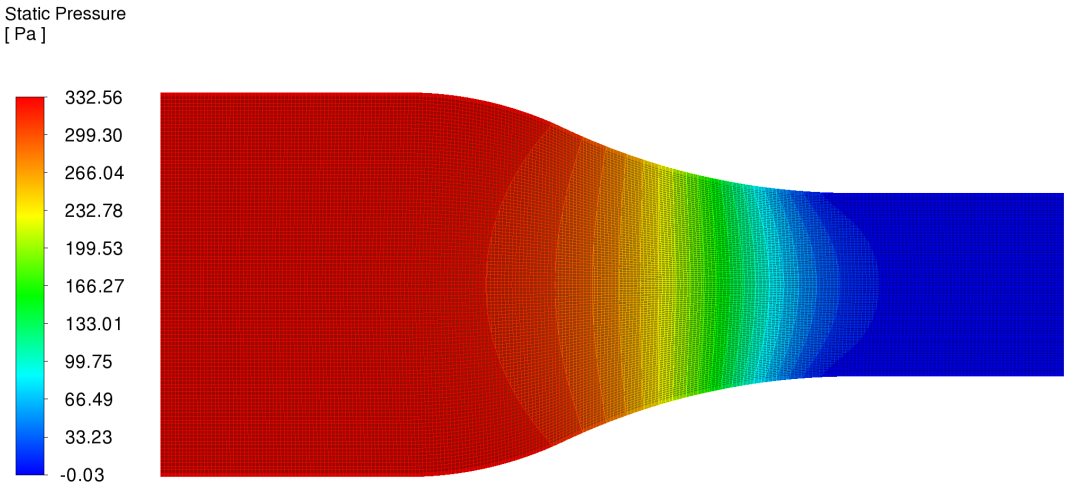

(e) Pressure of air at 5 m/s

Figure 3. Contour of pressure of air

According to Bernoulli's principle, the pressure drop in the converging section indicates that the fluid is accelerating, while the pressure increase in the diverging section indicates fluid deceleration. At higher speeds, the pressure distribution shows a more significant drop in the converging section, corresponding to the increased flow velocity that causes a more significant pressure drop. The pressure change is more gradual at lower speeds but follows the same pattern. In real-world conditions, viscosity affects the pressure distribution, especially near the nozzle walls. Therefore, it is essential to consider viscosity for practical analysis, even though the overall distribution follows Bernoulli's principle.

The pressure distribution in the converging-diverging nozzle reflects the basic principle of fluid flow, where acceleration causes a pressure drop, and deceleration causes a pressure increase. Increased airflow velocity shows a more significant pressure drop in the converging section. These results emphasize the importance of considering velocity and viscosity in fluid flow analysis for practical applications.

4.1.2 Velocity of air

Based on the velocity contour plots of air flowing through a converging-diverging nozzle at various inlet velocities (1 m/s, 2 m/s, 3 m/s, 4 m/s, and 5 m/s), as shown in Figure 4, a comprehensive analysis of how different inlet conditions influence air speed and pressure distribution can be derived. The figure illustrates the static pressure distribution within the nozzle, with red indicating higher pressure and blue indicating lower pressure, ranging from 1.00 Pa to 16.12 Pa.

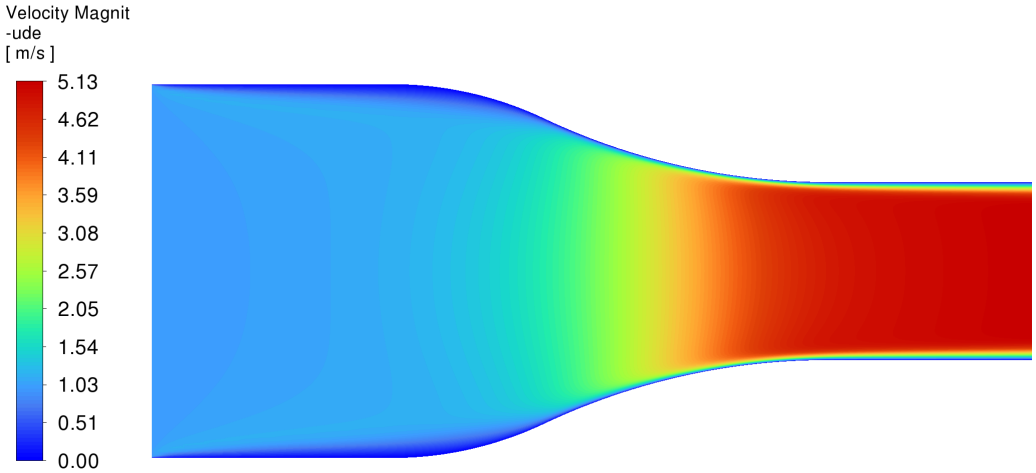

(a) Velocity of air at 1 m/s

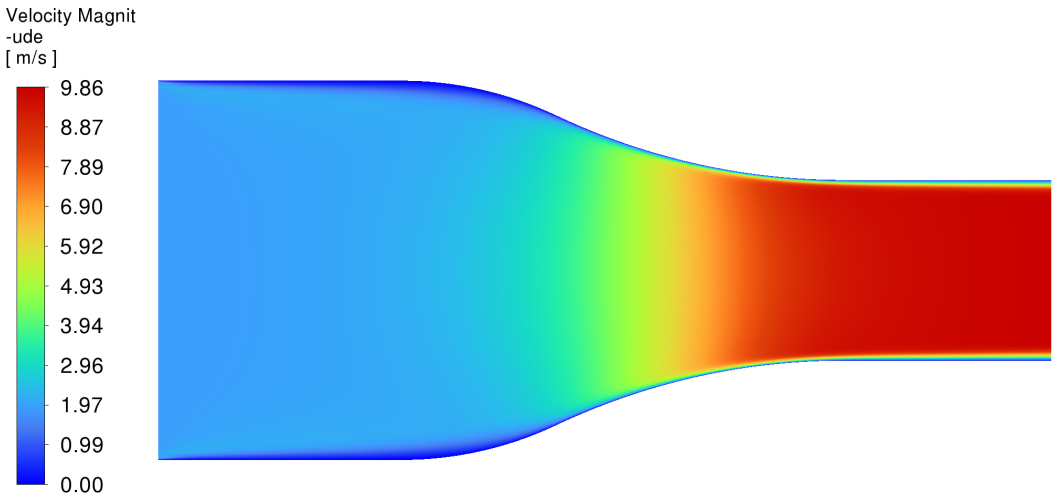

(b) Velocity of air at 2 m/s

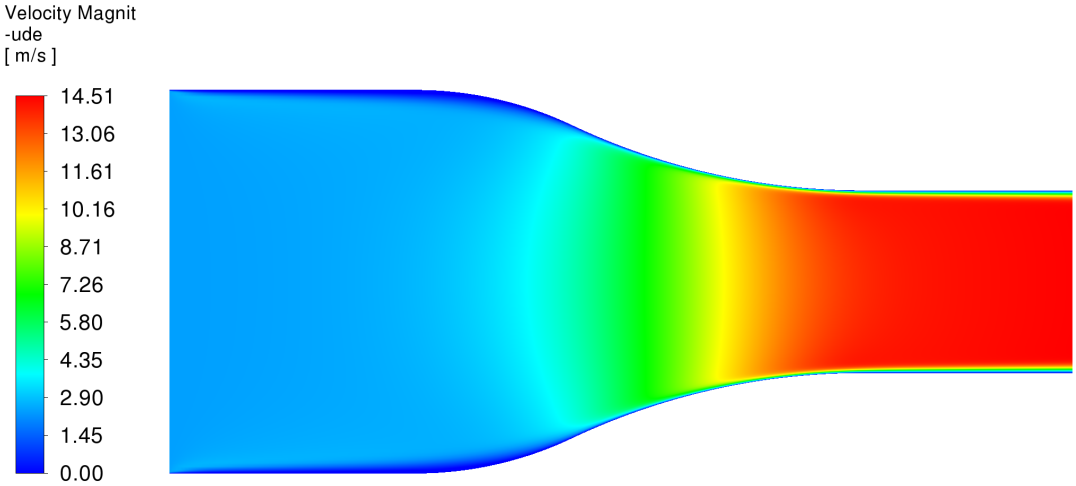

(c) Velocity of air at 3 m/s

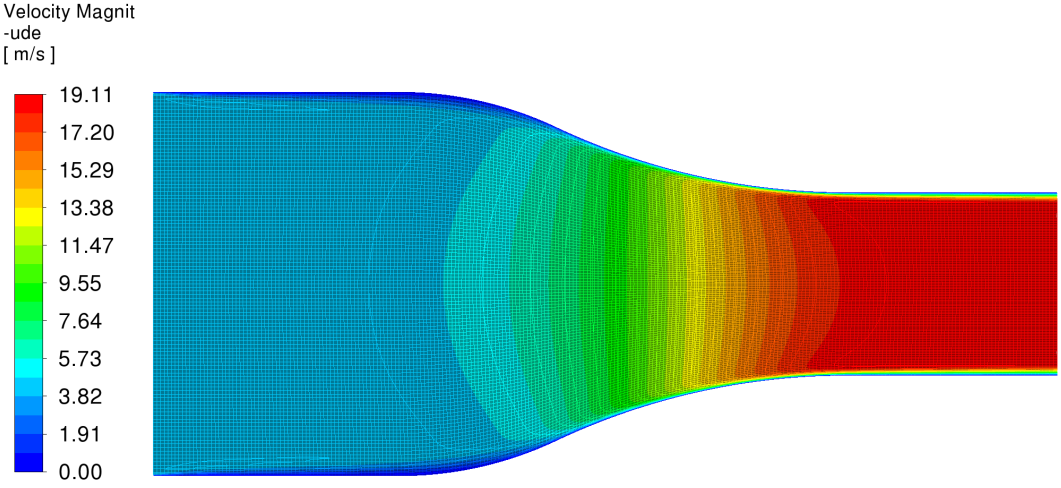

(d) Velocity of air at 4 m/s

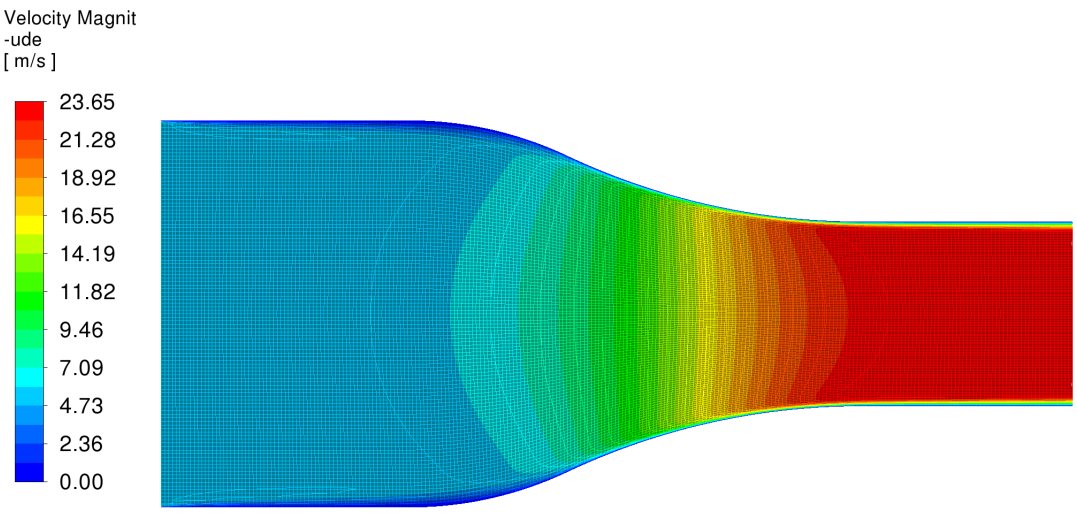

(e) Velocity of air at 5 m/s

Figure 4. Contour of velocity of air

At the inlet section, the air enters the nozzle at a relatively low speed of 1 m/s, marked by a blue color. As the inlet velocity increases from 2 m/s to 5 m/s, the initial pressure remains high, but the pressure drop becomes more pronounced in the converging section. This pressure drop results from the air acceleration, as observed by the color transition from blue to green to yellow and red at the narrowest section, where the maximum velocity is achieved. At higher inlet velocities, such as 5 m/s, the acceleration is much more significant, with the red area dominating, indicating substantial acceleration.

The air begins to decelerate in the diverging section, marked by the color change from red back to green and blue. The pressure increases again for all speeds, more noticeable at lower velocities. This pattern aligns with Bernoulli's principle, where an increase in fluid speed leads to a decrease in pressure and vice versa.

These velocity contour plots demonstrate the efficiency of the converging-diverging nozzle design in controlling airflow to achieve maximum velocity at the narrowest point. The design effectively showcases how increased inlet velocity corresponds to a higher maximum velocity within the nozzle. The overall distribution follows Bernoulli's principle, emphasizing the importance of considering initial velocity and viscosity for practical fluid flow applications.

4.1.3 Pressure of hydrogen

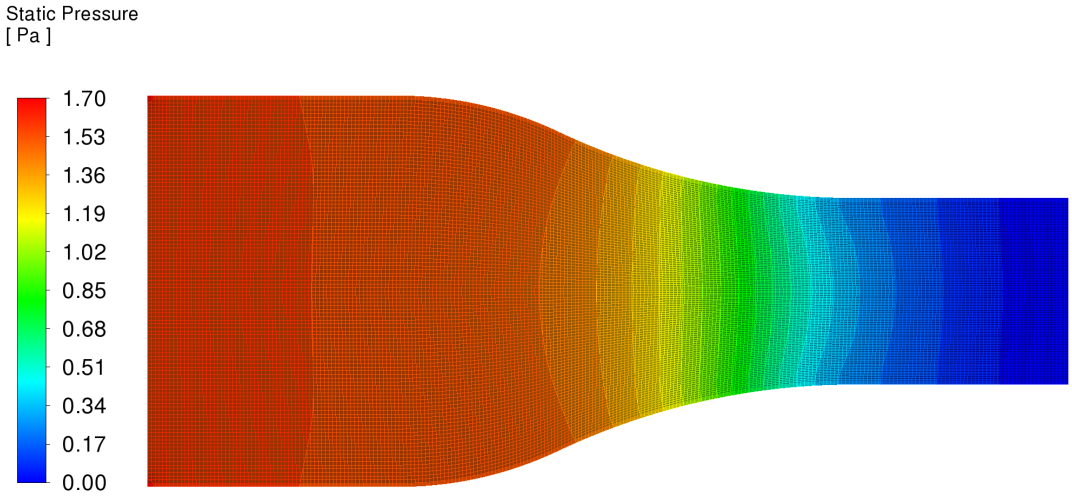

(a) Pressure of hydrogen at 1 m/s

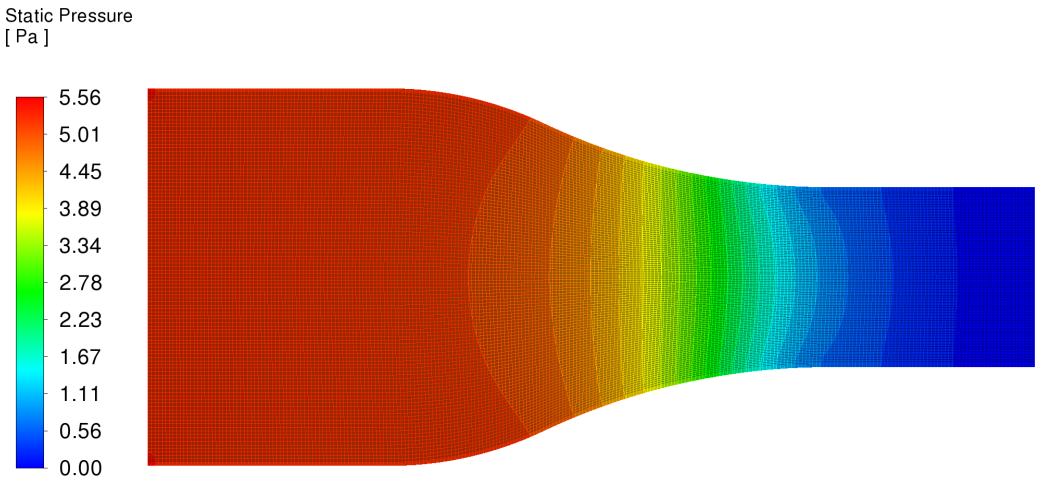

(b) Pressure of hydrogen at 2 m/s

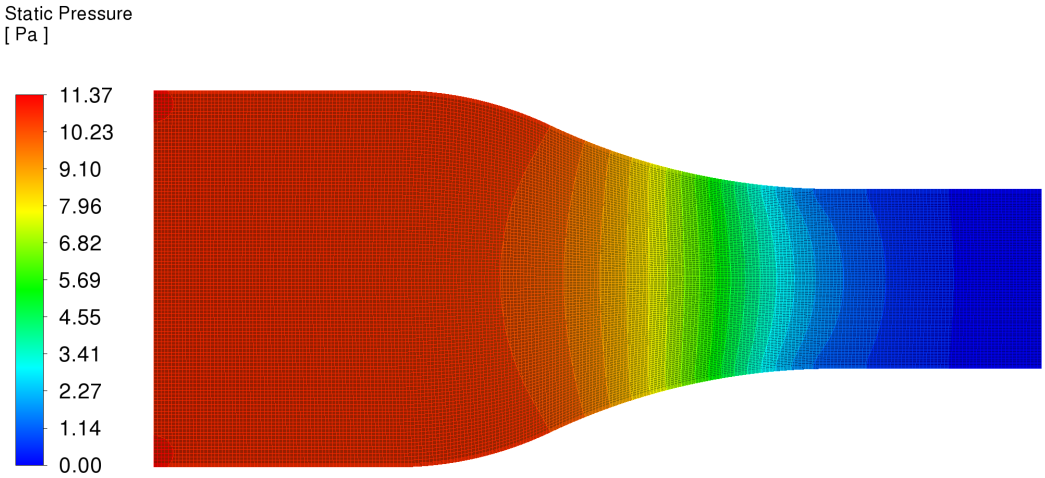

(c) Pressure of hydrogen at 3 m/s

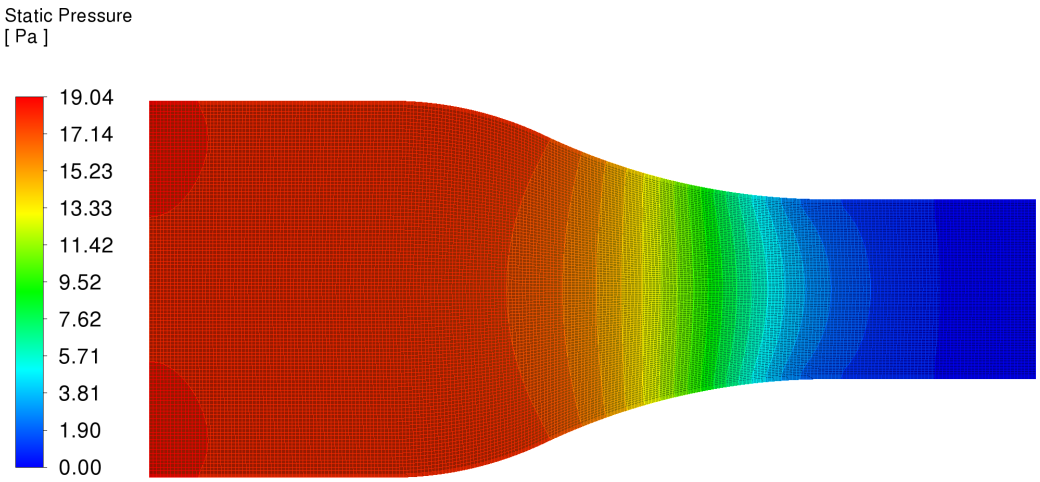

(d) Pressure of hydrogen at 4 m/s

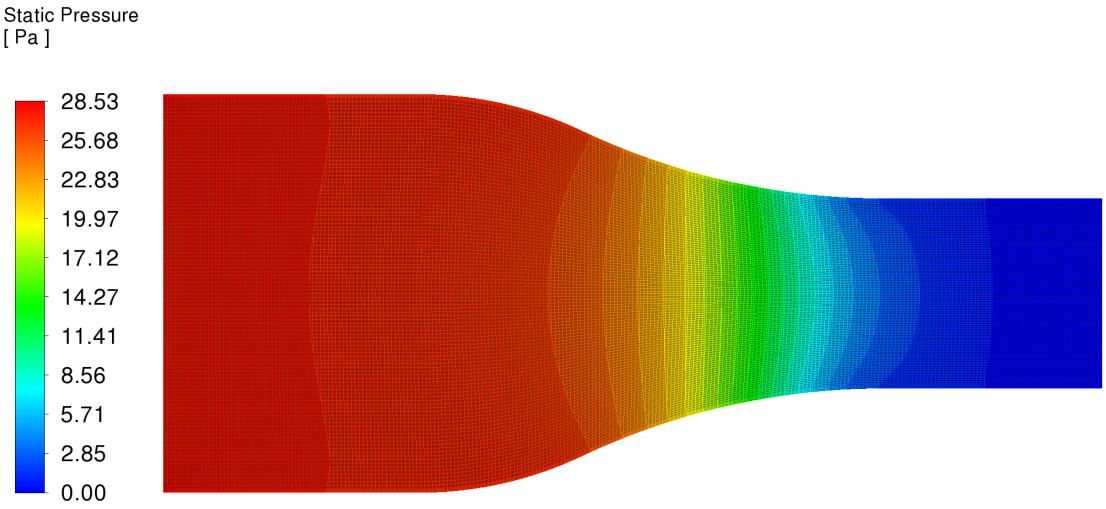

(e) Pressure of hydrogen at 5 m/s

Figure 5. Contour of pressure of hydrogen

Figure 5 shows the contour plots of static pressure distribution for hydrogen gas flowing through a converging-diverging nozzle at various inlet velocities (1 m/s, 2 m/s, 3 m/s, 4 m/s, and 5 m/s) and reveals insightful details about how the pressure distribution is affected by different flow conditions. The plots indicate that at the lowest inlet velocity of 1 m/s, the pressure distribution is relatively uniform with a moderate pressure gradient. As the inlet velocity increases to 2 m/s, a more pronounced pressure drop is observed, with a steeper gradient. At 3 m/s, the pressure drop becomes even more significant, highlighting intense acceleration and a resulting pressure decrease. At 4 m/s and 5 m/s, the static pressure distribution shows dramatic pressure drops with the steepest gradients, emphasizing substantial acceleration as the hydrogen gas passes through the nozzle. These results align with Bernoulli's principle, demonstrating that an increase in gas velocity corresponds with a decrease in pressure. The efficiency of the converging-diverging nozzle design in accelerating hydrogen gas is evident, facilitating significant increases in flow speed while reducing pressure at the throat. This analysis underscores the importance of considering velocity and pressure changes in nozzle design to optimize performance in practical gas flow applications.

4.1.4 Velocity of hydrogen

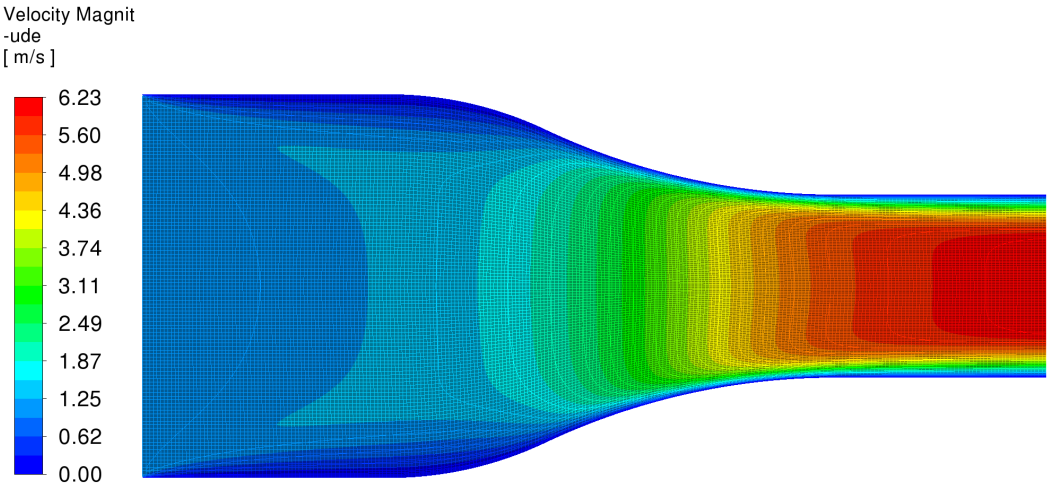

(a) Velocity of hydrogen at 1 m/s

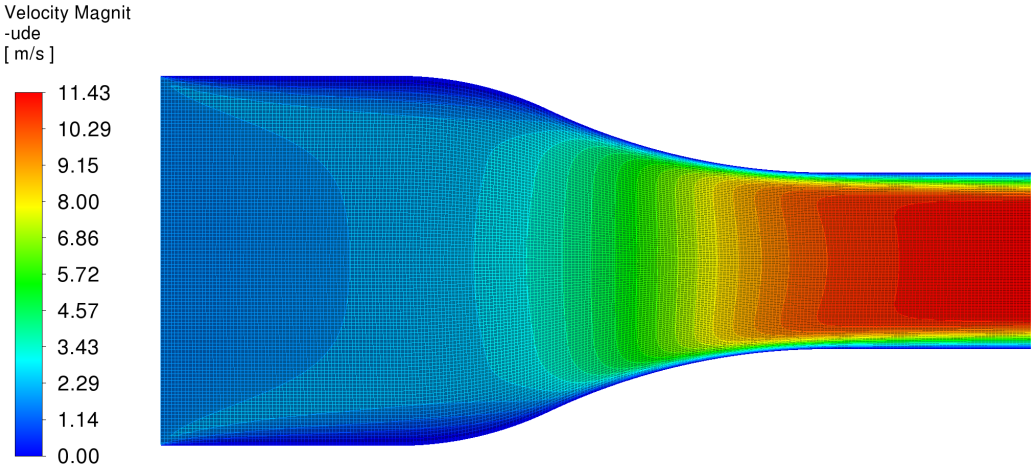

(b) Velocity of hydrogen at 2 m/s

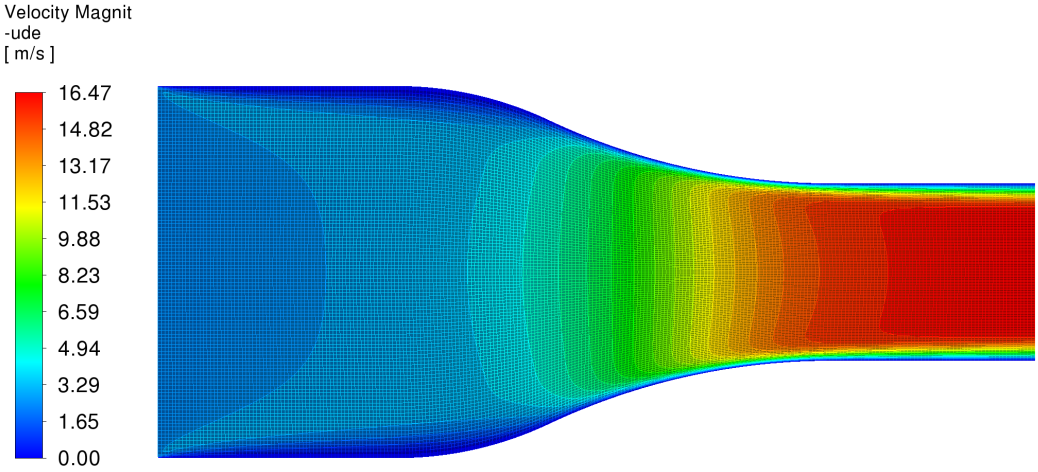

(c) Velocity of hydrogen at 3 m/s

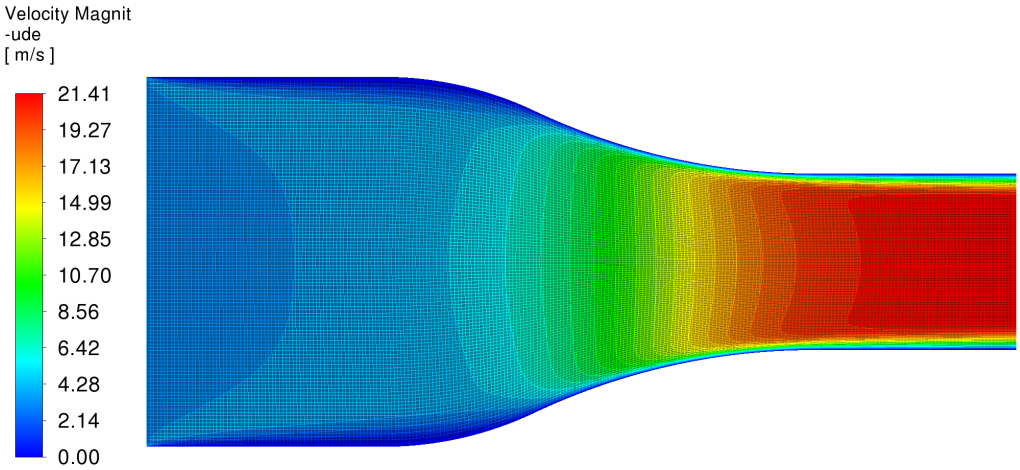

(d) Velocity of hydrogen at 4 m/s

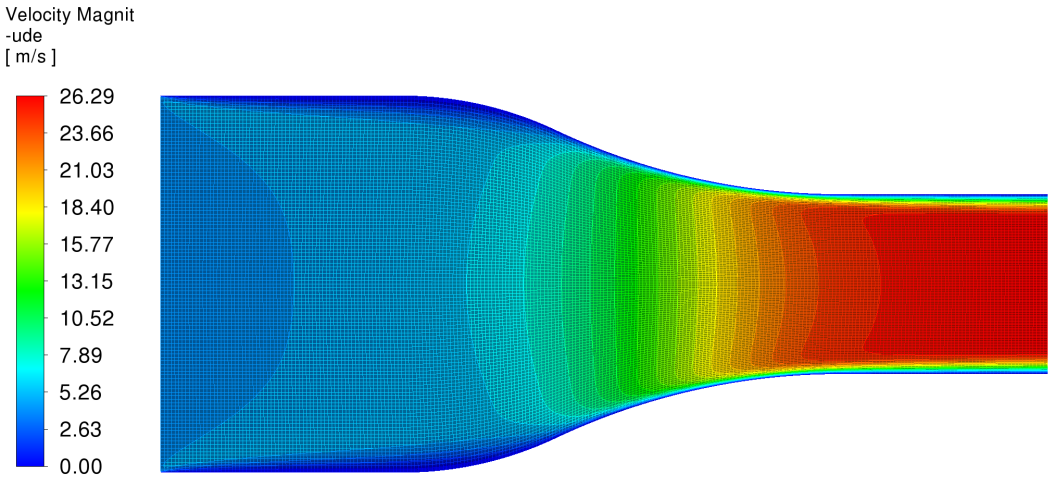

(e) Velocity of hydrogen at 5 m/s

Figure 6. Contour of velocity of hydrogen

Figure 6 shows this simulation of hydrogen flow through a channel with a converging section at varying inlet velocities (1 m/s to 5 m/s), revealing a consistent flow pattern where the fluid velocity increases significantly in the constricted region, as dictated by the continuity equation. In the larger cross-sectional area, the flow exhibits low velocity, represented by blue regions, while the maximum velocity is observed in the constriction, highlighted in red. The maximum velocity increases linearly with the inlet velocity, ranging from approximately 6.22 m/s at 1 m/s inlet velocity to 26.29 m/s at 5 m/s. This behavior reflects the direct proportionality between the fluid's inlet velocity and kinetic energy.

The velocity distribution also corroborates Bernoulli's principle, where the static pressure decreases as the fluid velocity increases. The highest pressure occurs in the larger cross-sectional area with lower velocity, while the lowest pressure is found in the constricted region with higher velocity. Furthermore, the increase in inlet velocity leads to a rise in the Reynolds number, indicating a potential transition from laminar to turbulent flow, particularly at higher inlet velocities such as 4 m/s and 5 m/s.

This phenomenon illustrates the Venturi effect, where a reduction in cross-sectional area causes a significant increase in fluid velocity and a corresponding pressure drop. The simulation is highly relevant for the design of hydrogen flow systems, such as Venturi meters, nozzles, and pipelines, as well as other applications that leverage velocity and pressure variations in fluid dynamics. The increase in kinetic energy within the constricted region highlights the importance of controlling the inlet velocity to ensure flow stability and avoid conditions such as turbulence or cavitation.

4.1.5 Pressure of helium

Figure 7 shows the fluid flow in the nozzle using helium as the working fluid, showing an interesting interaction between the fluid velocity and the resulting static pressure. At a velocity magnitude of 1 m/s and 2 m/s, have static pressure values of 3.59 and 11.57. This indicates that the pressure inside the nozzle is relatively low at low velocities, allowing the helium to flow with a relatively constant pressure. This indicates that at this speed range, there is a point where increasing the speed does not significantly change the static pressure, likely due to the dynamic stability in the pressure distribution in the nozzle.

When the fluid velocity reaches 3 m/s, there is a jump in the highest static pressure to 23.48. This spike can be explained by the increase in the fluid's kinetic energy, which directly affects the static pressure inside the nozzle. This increase indicates that the nozzle encounters more dynamic flow changes, where kinetic energy contributes significantly to the overall pressure. At a velocity of 4 m/s, the static pressure increases more drastically to 39.16. This change indicates that the nozzle's flow rate and turbulence effects are becoming more significant. The increase in fluid velocity increases pressure due to the higher acceleration of the helium particles.

Furthermore, when the velocity reaches 5 m/s, the static pressure reaches 58.51. This figure reflects that the nozzle experiences more significant static pressure at high speeds due to the increased friction force and higher fluid flow velocity. This effect demonstrates the complexity of the turbulent flow inside the nozzle, where high velocities

lead to a more volatile and diverse pressure distribution.

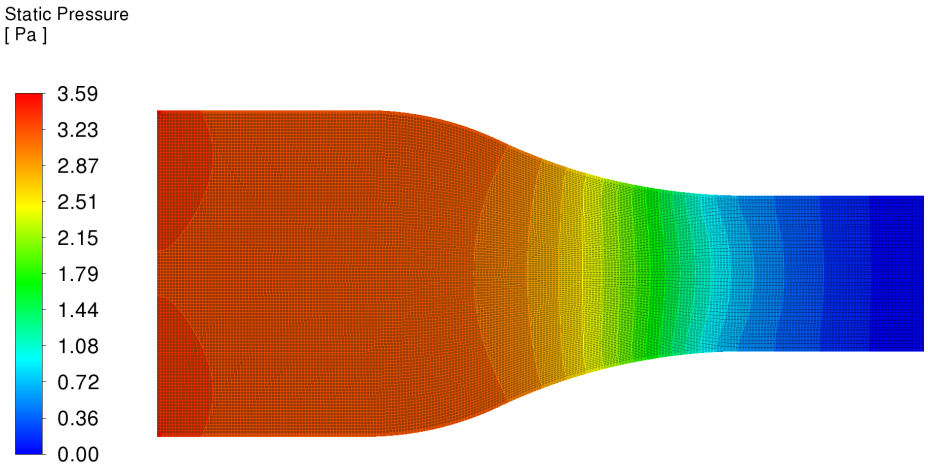

(a) Pressure of helium at 1 m/s

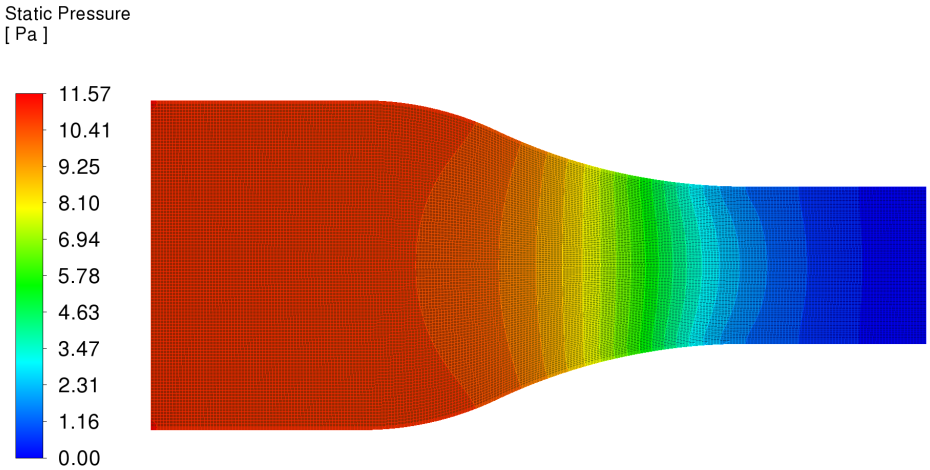

(b) Pressure of helium at 2 m/s

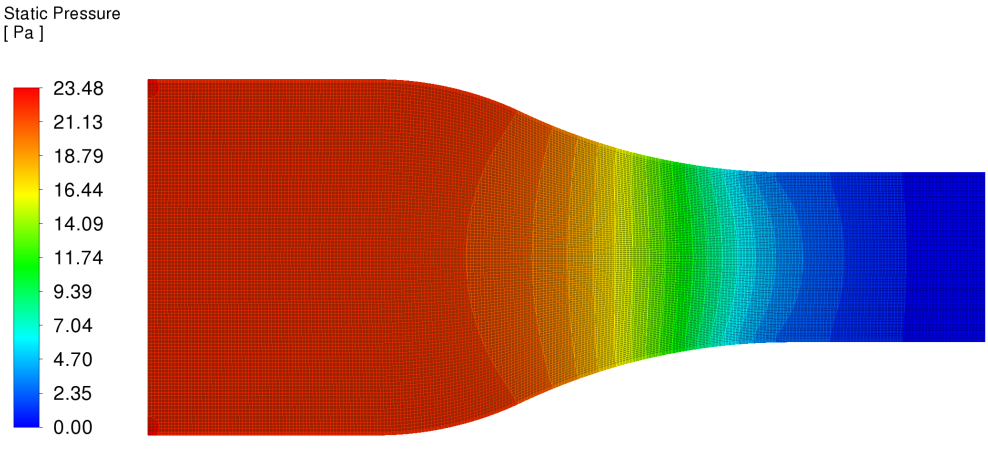

(c) Pressure of helium at 3 m/s

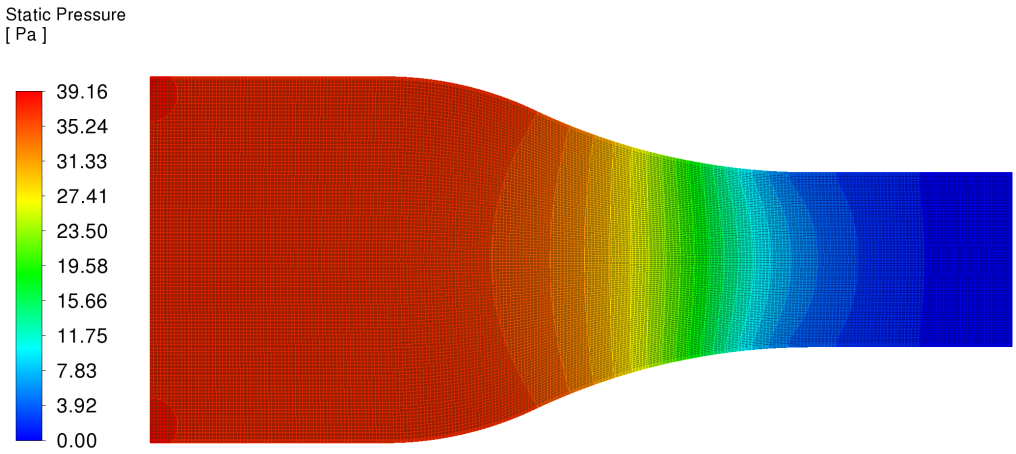

(d) Pressure of helium at 4 m/s

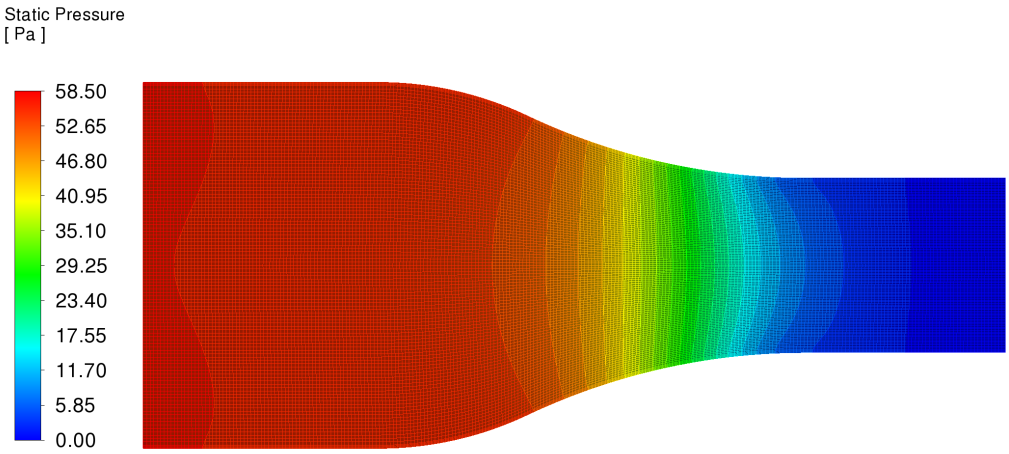

(e) Pressure of helium at 5 m/s

Figure 7. Contour of pressure of helium

Overall, this analysis illustrates how velocity variations within the nozzle affect the static pressure of helium. The pressure changes are insignificant at low speeds. But at higher speeds, the static pressure increases dramatically, reflecting the complex interplay between velocity and fluid flow dynamics in the nozzle. This increase demonstrates the need for nozzle designs that consider velocity variations to optimize flow performance and prevent the occurrence of overpressure effects that can damage the nozzle structure.

4.1.6 Velocity of helium

Below are the results of static pressure and inlet velocity on the viscous and inviscid contours.

Figure 8 shows the helium flow through a nozzle at varying inlet velocities (1 m/s to 5 m/s), revealing a linear relationship between the inlet velocity and the maximum velocity magnitude achieved within the nozzle. At an inlet velocity of 1 m/s, the maximum velocity magnitude is recorded at 6.38 m/s. This value increases progressively as the inlet velocity rises, with maximum velocity magnitudes of 16.47 m/s at 3 m/s inlet velocity, 21.41 m/s at 4 m/s, and 26.29 m/s at 5 m/s. These results are consistent with fluid dynamics principles, precisely the continuity equation and energy conservation, which govern the behavior of compressible and incompressible flows through constrictions.

The nozzle geometry largely determines the relationship between the inlet velocity and the maximum velocity magnitude. The converging section of the nozzle accelerates the flow as the cross-sectional area decreases, leading to a higher velocity magnitude downstream. This phenomenon is particularly evident in helium, a light and highly diffusive gas that responds significantly to pressure and velocity field changes. The proportional increase in maximum velocity magnitude with the inlet velocity aligns with the law of conservation of mass, as the product of velocity and

cross-sectional area remains constant throughout the nozzle.

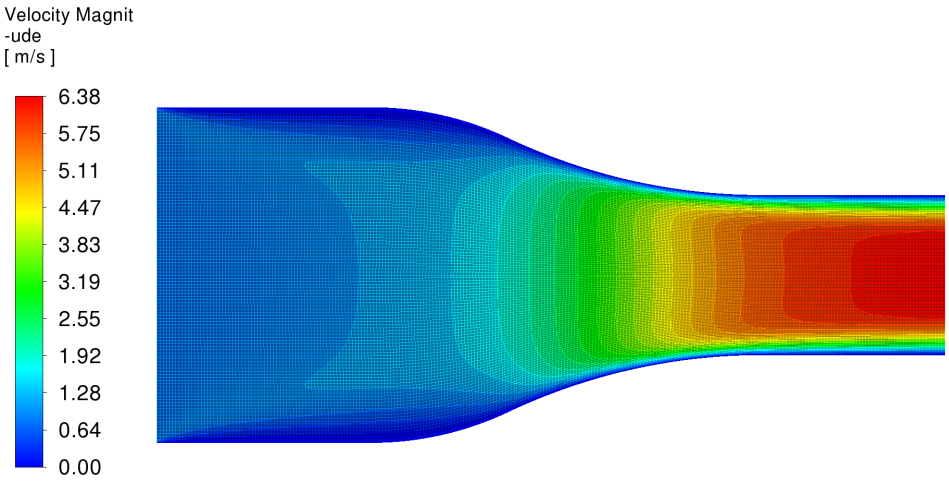

(a) Velocity of helium at 1 m/s

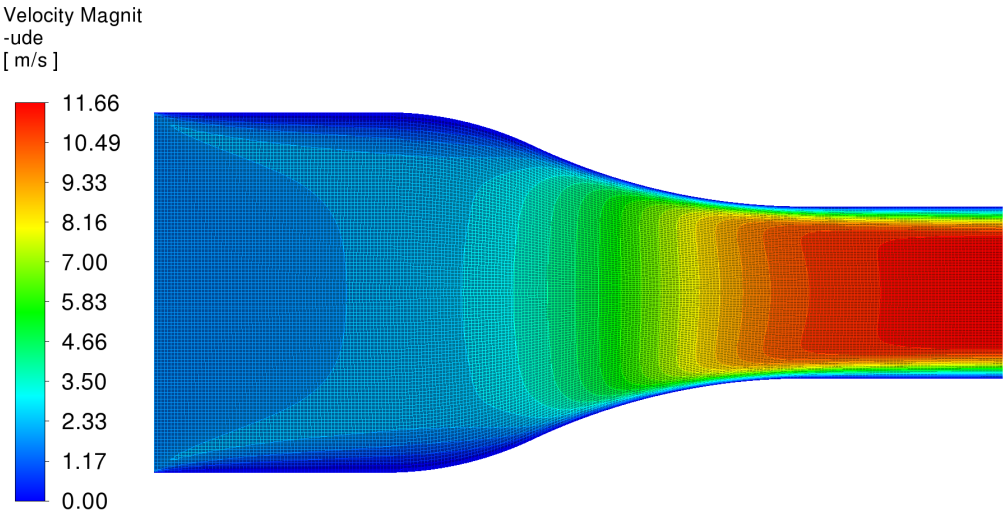

(b) Velocity of helium at 2 m/s

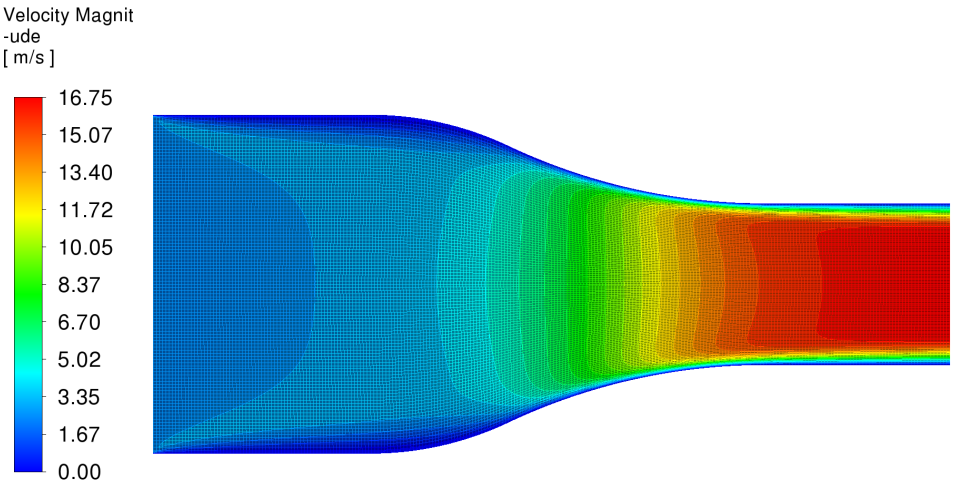

(c) Velocity of helium at 3 m/s

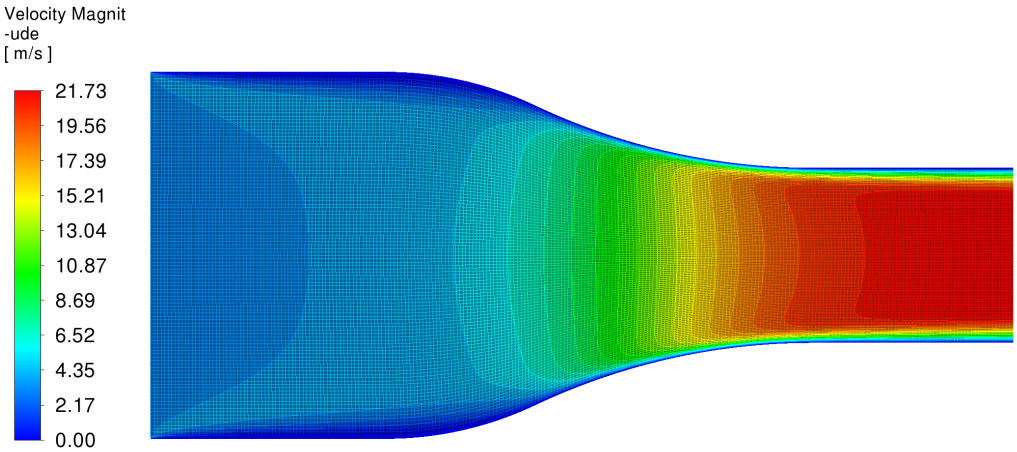

(d) Velocity of helium at 4 m/s

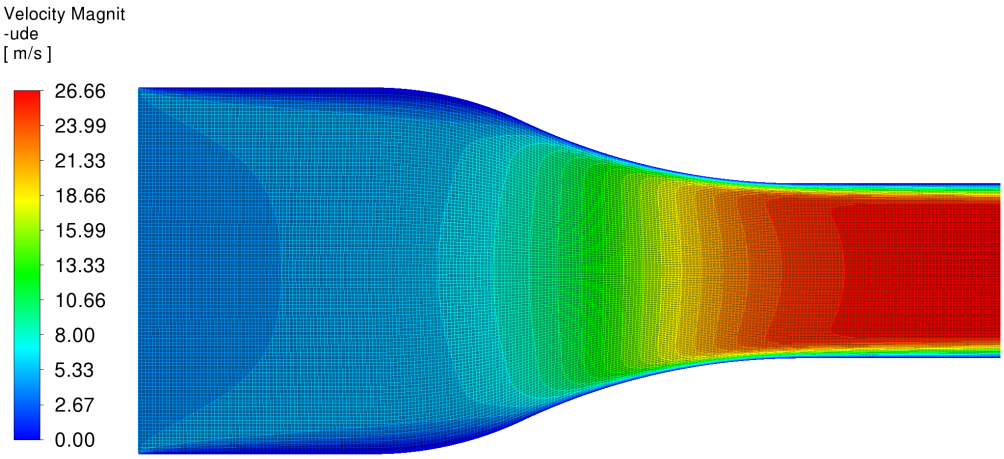

(e) Velocity of helium at 5 m/s

Figure 8. Contour of velocity of helium

As Bernoulli's principle describes, the increase in velocity magnitude also highlights the conversion of pressure energy into kinetic energy. At higher inlet velocities, a more significant proportion of the fluid's total energy is directed toward increasing the kinetic energy, resulting in higher velocities in the nozzle's throat and divergent section. This behavior is crucial for applications where helium is used, such as in propulsion systems, cryogenic cooling, or industrial gas delivery, as it underscores the importance of controlling inlet velocities to achieve desired flow properties.

The near-linear trend in velocity magnitude also indicates that the flow remains within a regime where compressibility effects are minimal, at least at the given velocities. However, the transition to supersonic or compressible flow may occur at higher velocities, introducing nonlinearities into the velocity-pressure relationship. This analysis highlights the need for precise nozzle design to optimize helium flow for specific industrial or scientific applications, ensuring efficient energy conversion and flow management.

4.2 Inviscid

4.2.1 Pressure of air

Below are the results of static pressure and inlet velocity on the viscous and inviscid contours.

Figure 9 shows fluid flow within a convergent-divergent nozzle using helium as the working fluid, revealing a significant relationship between fluid velocity and the resulting static pressure. At a liquid velocity of 1 m/s, the highest static pressure recorded is 11.57. At this stage, the flow tends to be stable with minimal variation in pressure distribution. When the fluid velocity increases to 2 m/s, the highest static pressure remains at 11.57, indicating pressure stability within the nozzle despite the increase in velocity. This stability may be attributed to the dynamic characteristics of helium flow under low-velocity conditions, where the change in velocity is not substantial enough to

cause a drastic change in pressure.

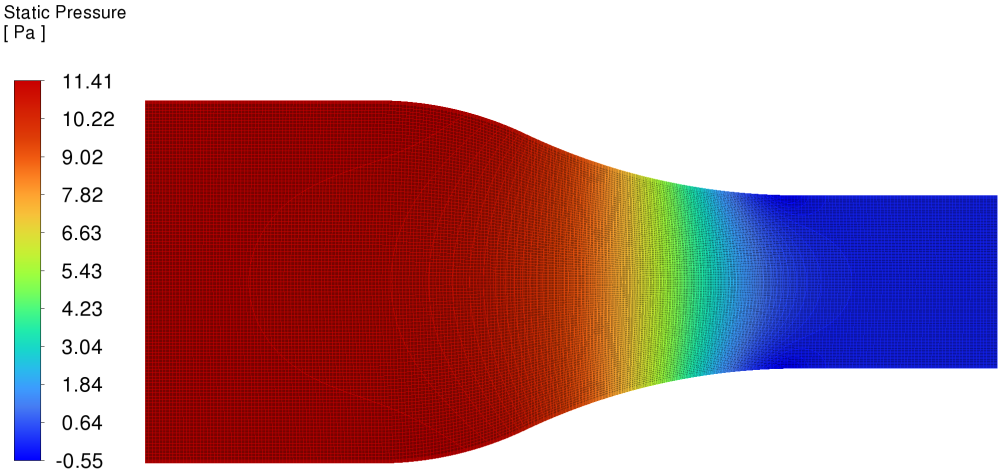

(a) Pressure of air at 1 m/s

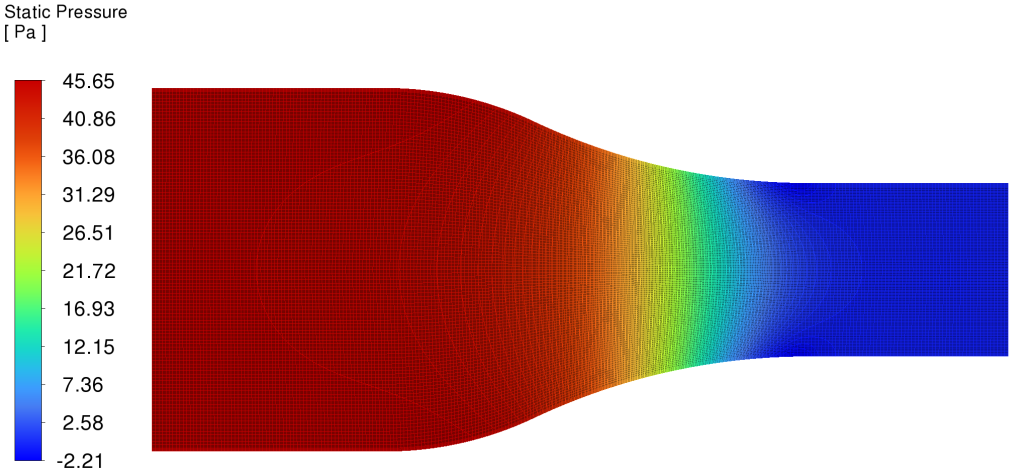

(b) Pressure of air at 2 m/s

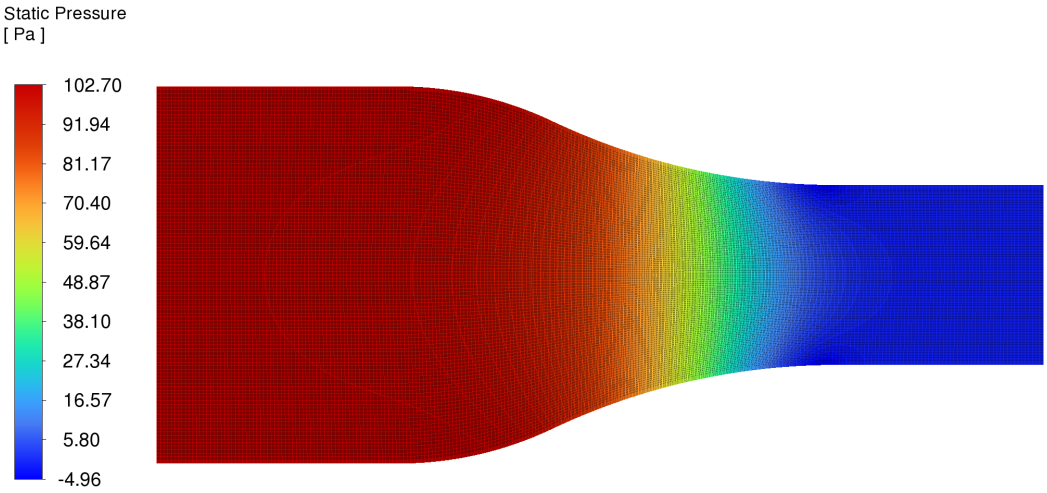

(c) Pressure of air at 3 m/s

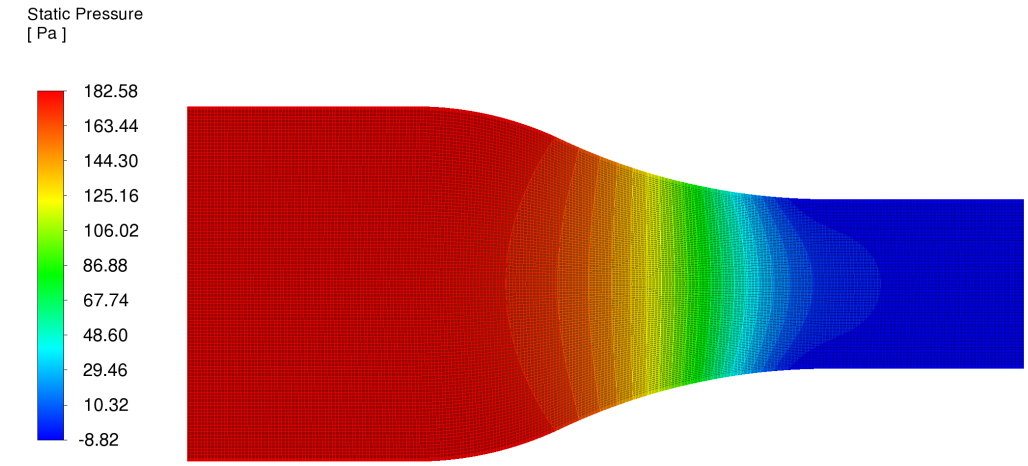

(d) Pressure of air at 4 m/s

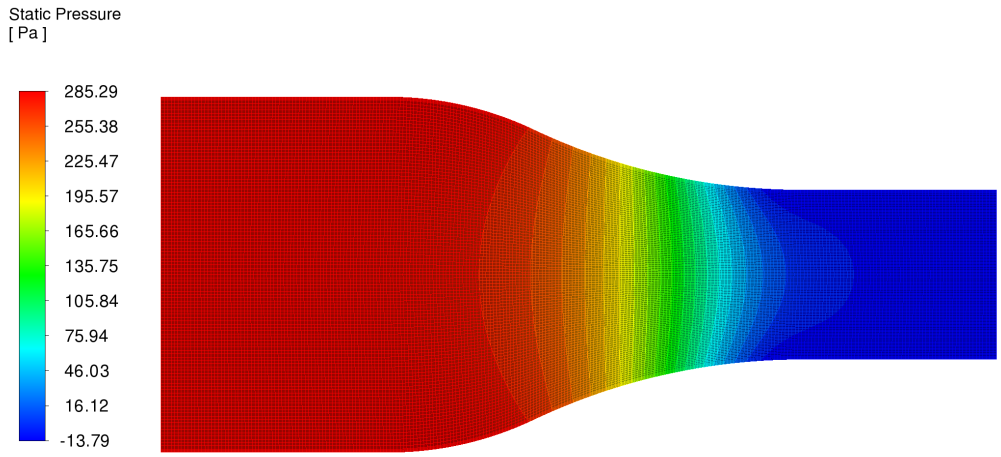

(e) Pressure of air at 5 m/s

Figure 9. Contour of pressure of air

However, as the velocity increases to 3 m/s, there is a surge in static pressure to 23.48. This increase can be explained by the rise in kinetic energy of the fluid, resulting in higher static pressure within the nozzle. This phenomenon reflects the transition from a more laminar flow to a more turbulent one, where kinetic energy dominates pressure distribution. At a velocity of 4 m/s, the static pressure rises sharply to 39.16. This increase indicates a more dynamic interaction between the helium flow and the nozzle structure. The higher acceleration of helium particles leads to a more significant increase in static pressure, reflecting the influence of flow acceleration on pressure within the nozzle.

Furthermore, at a velocity of 5 m/s, the static pressure increases to 58.51. At this velocity, the flow within the nozzle is in a highly dynamic state with more fluctuating pressure distribution. The significant pressure increase indicates that the nozzle experiences greater turbulence, where helium particles move at high speeds and cause higher static pressure. This also shows that the frictional effects within the nozzle at high velocities become more significant, contributing to the increase in static pressure.

Overall, this analysis demonstrates how variations in velocity within the nozzle affect the static pressure of helium. At low velocities, the change in pressure is not significant. Still, at higher velocities, the static pressure increases dramatically, reflecting the complex interaction between velocity and fluid dynamics within the nozzle. This increase underscores the importance of nozzle design that considers velocity variations to optimize flow performance and prevent excessive pressure that could damage the nozzle structure. By understanding the flow dynamics and static pressure changes at various velocities, the nozzle design and performance in practical applications can be optimized, ensuring better operational efficiency and sustainability.

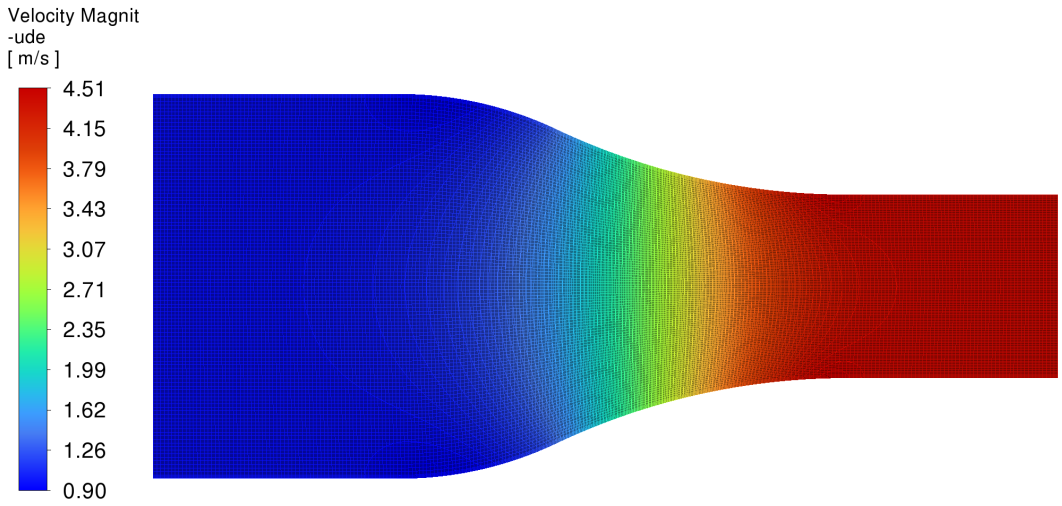

(a) Velocity of air at 1 m/s

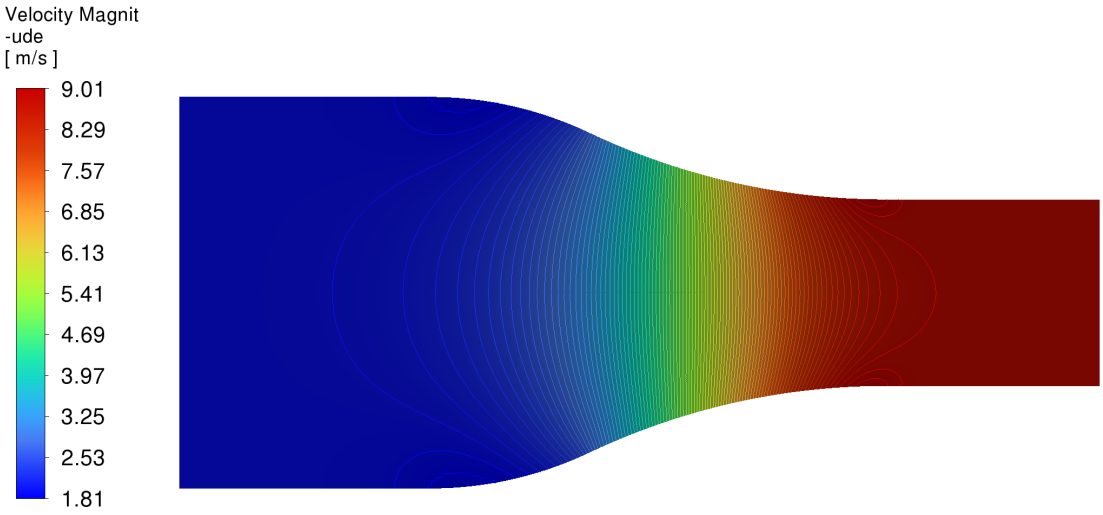

(b) Velocity of air at 2 m/s

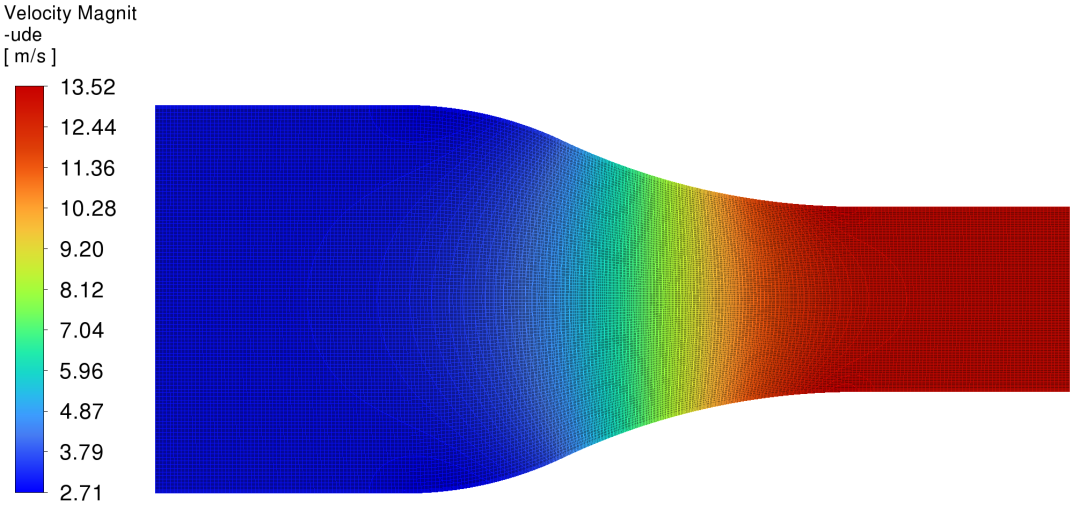

(c) Velocity of air at 3 m/s

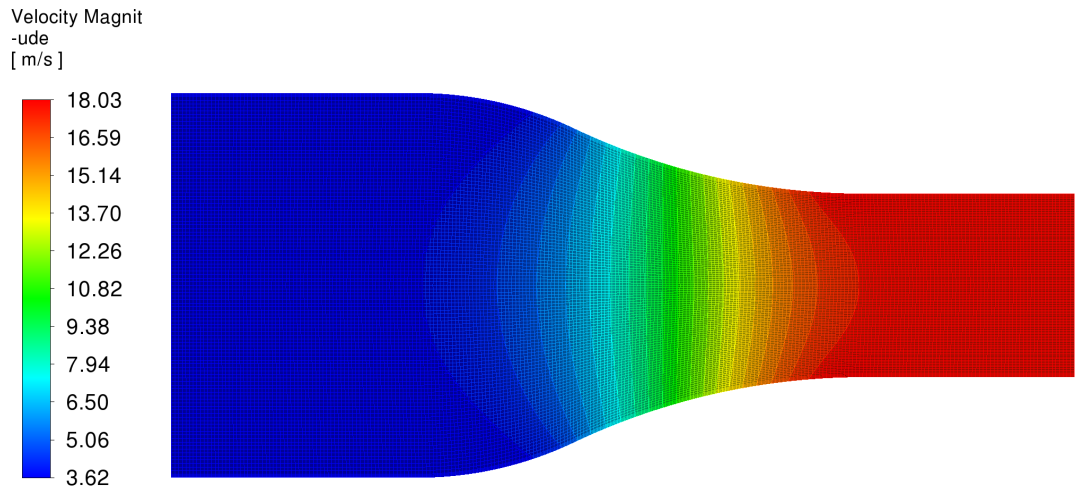

(d) Velocity of air at 4 m/s

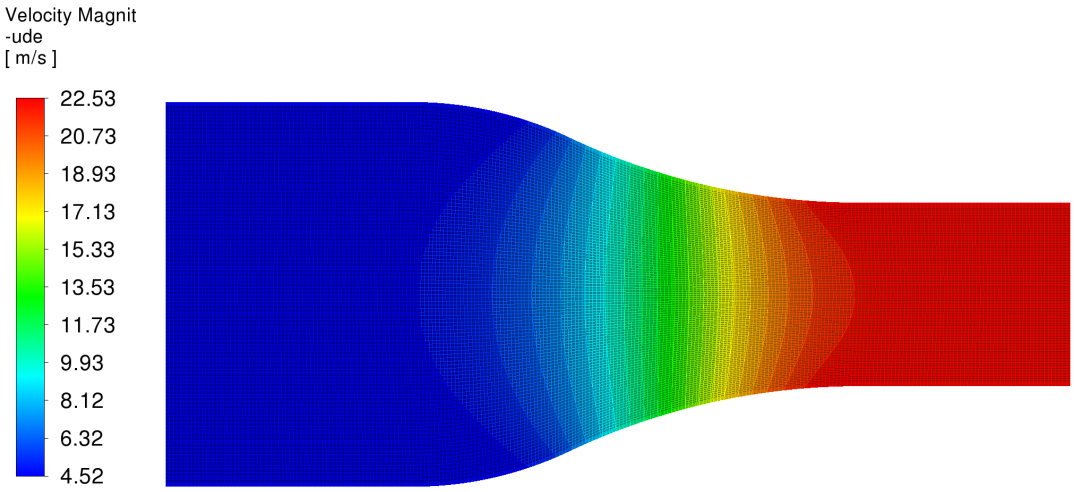

(e) Velocity of air at 5 m/s

Figure 10. Contour of velocity of air

4.2.2 Velocity of air

Figure 10 presents a detailed analysis of velocity magnitude distributions within a converging-diverging nozzle at different inlet velocities, showcasing airflow behavior under varying conditions. Initially, at a lower inlet velocity of 1 m/s, the contour plot demonstrates a gradual increase in velocity towards the nozzle's throat, where the velocity peaks due to the Venturi effect. The color gradient transitions from blue, indicating lower velocities, to red, indicating higher velocities, with the highest velocity around 4.51 m/s. As the inlet velocity increases to 2 m/s, the airflow accelerates more significantly at the nozzle throat, peaking at approximately 9.01 m/s. This more dynamic flow is highlighted by the broader range of high-velocity regions in the color gradient, reflecting the impact of increased kinetic energy on velocity distribution.

Further analysis is provided by the additional contour plots at inlet velocities of 3 m/s, 4 m/s, and 5 m/s. At 3 m/s, the velocity magnitude ranges from 2.71 m/s to 13.52 m/s, showing a pronounced acceleration at the throat. At 4 m/s, the velocity range extends from 3.62 m/s to 18.00 m/s, indicating a more significant increase in velocity through the nozzle. The highest inlet velocity of 5 m/s results in velocity magnitudes ranging from 4.52 m/s to 20.73 m/s, with the most substantial acceleration observed at the nozzle's throat, highlighted by the dominant red regions in the plot.

This comprehensive analysis reveals crucial insights into how inlet velocity affects airflow characteristics within a converging-diverging nozzle. As the inlet velocity increases, the kinetic energy of the airflow rises, leading to higher peak velocities and more complex velocity distributions. Understanding these dynamics is vital for optimizing nozzle design in various engineering applications, such as propulsion systems, Heating, Ventilation and Air Conditioning

(HVAC) systems, and aerodynamic components. By analyzing the velocity distributions at different inlet velocities, engineers can enhance nozzle efficiency and performance, ensuring precise control over airflow to meet specific operational requirements. This combined analysis underscores the importance of considering velocity variations in nozzle design to achieve optimal functionality and avoid potential issues related to excessive pressure and turbulence.

4.2.3 Pressure of hydrogen

Figure 11 shows CFD simulations of hydrogen gas flowing through a converging-diverging nozzle at different inlet velocities, revealing critical insights into the behavior of compressible fluids under varying conditions.

Subgraph (a) of Figure 11 presents the static pressure distribution for hydrogen gas at an inlet velocity of 1 m/s. The pressure ranges from 0.04 to 0.76 Pa, dropping significantly at the throat due to the Venturi effect. The pressure then recovers as the gas exits the nozzle, transitioning from low to high pressure, indicating the influence of the nozzle's geometry on the flow dynamics.

Subgraphs (b) and (c) of Figure 11 provide contour plots at inlet velocities of 2 m/s and 3 m/s. For the 2 m/s flow, the pressure ranges show a notable decrease at the throat, followed by a slight increase at the nozzle's exit. At 3 m/s, the pressure variations become more pronounced, reflecting higher kinetic energy and dynamic behavior. The static pressure at the inlet is higher, resulting in a more significant drop at the throat and subsequent pressure recovery, highlighting the effect of increased inlet velocity on the pressure distribution.

Subgraphs (d) and (e) of Figure 11 illustrate pressure distributions at inlet velocities of 4 m/s and 5 m/s. At 4 m/s, the pressure ranges from 0.59 Pa to 12.21 Pa, dropping sharply at the throat and recovering in the divergent section. At 5 m/s, the pressure ranges from -0.92 Pa to 19.07 Pa, showing even more pronounced pressure variations. The increased inlet velocity leads to higher kinetic energy, causing a significant drop in pressure at the throat and a marked pressure recovery at the exit.

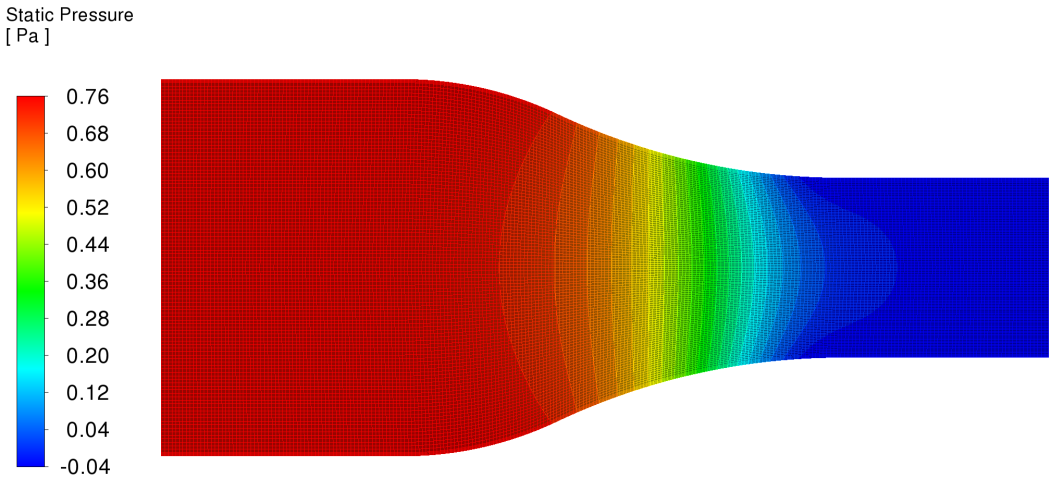

(a) Pressure of hydrogen at 1 m/s

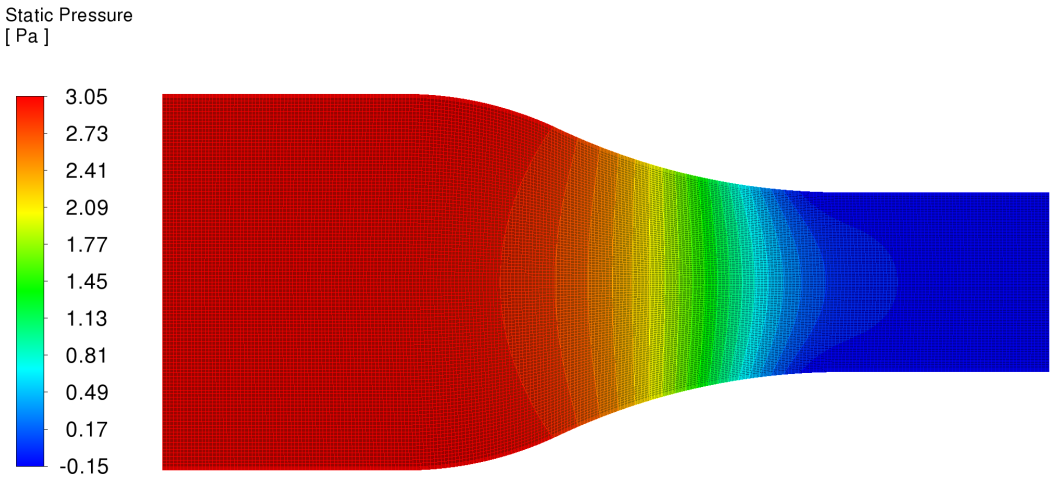

(b) Pressure of hydrogen at 2 m/s

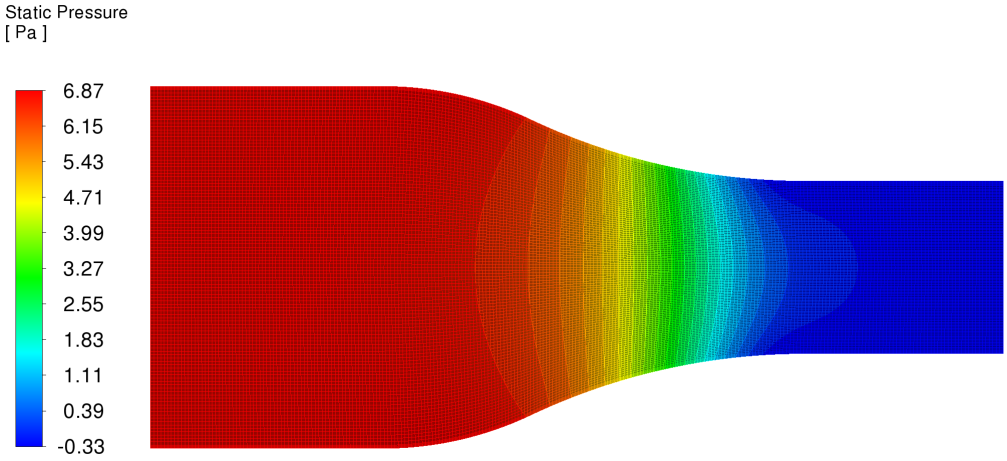

(c) Pressure of hydrogen at 3 m/s

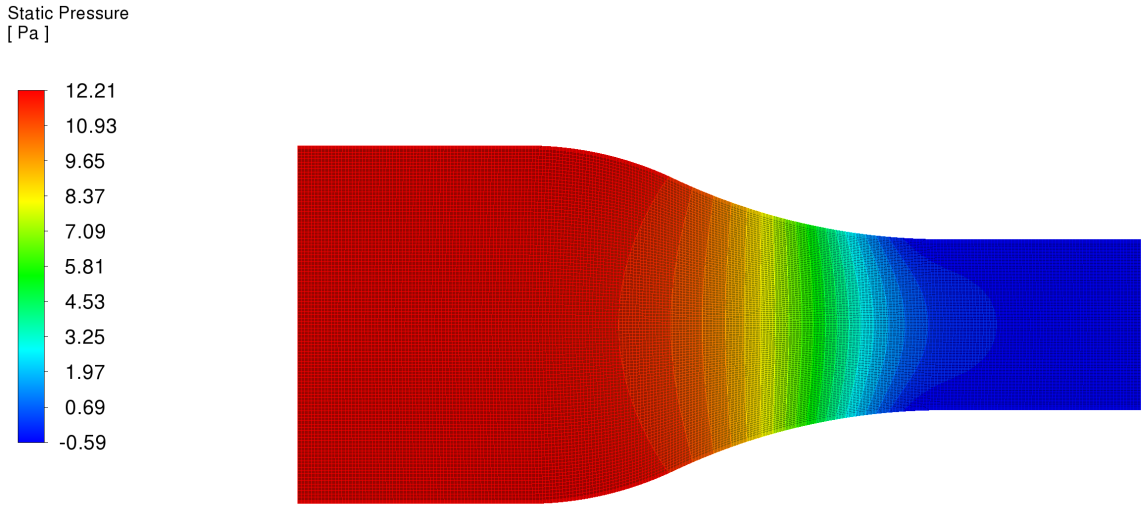

(d) Pressure of hydrogen at 4 m/s

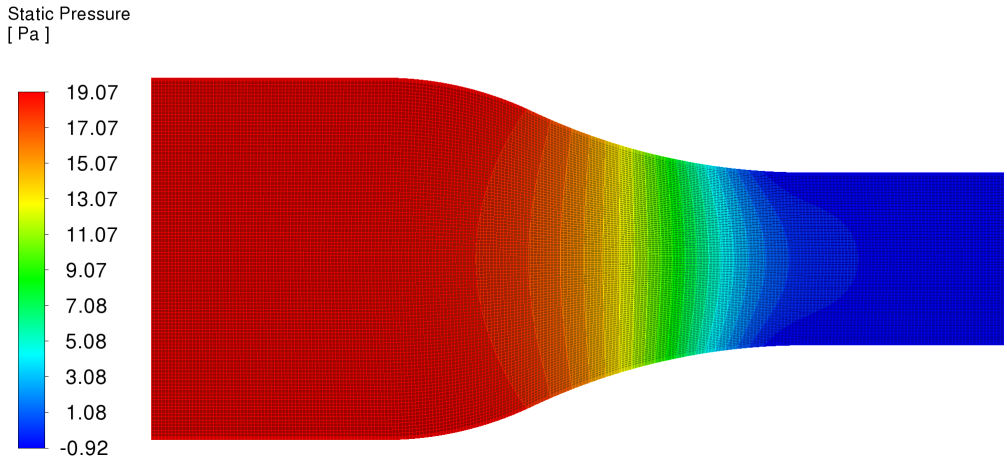

(e) Pressure of hydrogen at 5 m/s

Figure 11. Contour of pressure of hydrogen

By understanding the relationship between inlet velocity and static pressure distribution, engineers can design

nozzles that accommodate various flow conditions, enhancing the overall effectiveness and sustainability of engineering systems.

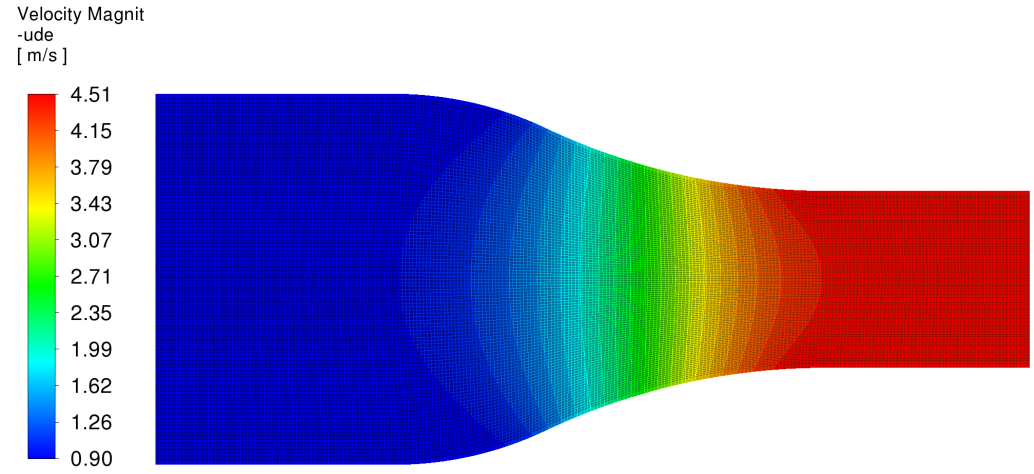

(a) Velocity of hydrogen at 1 m/s

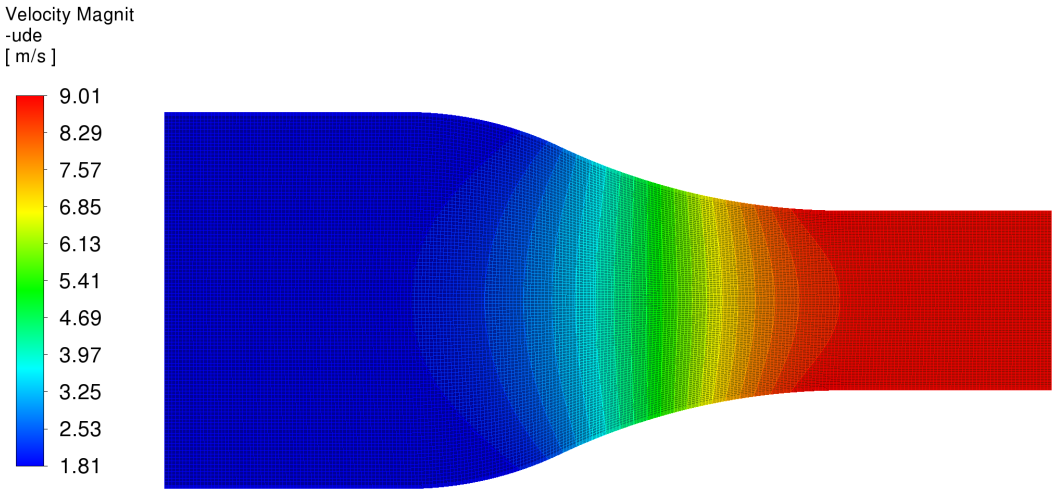

(b) Velocity of hydrogen at 2 m/s

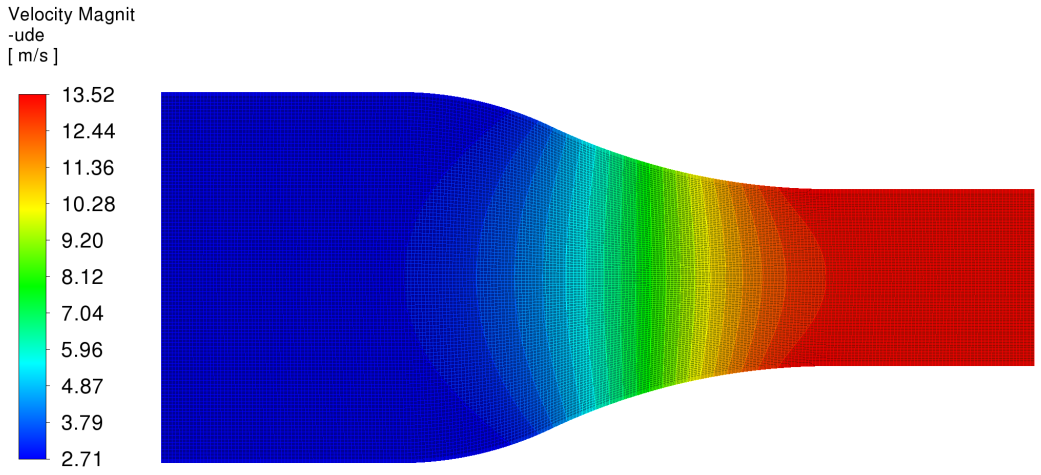

(c) Velocity of hydrogen at 3 m/s

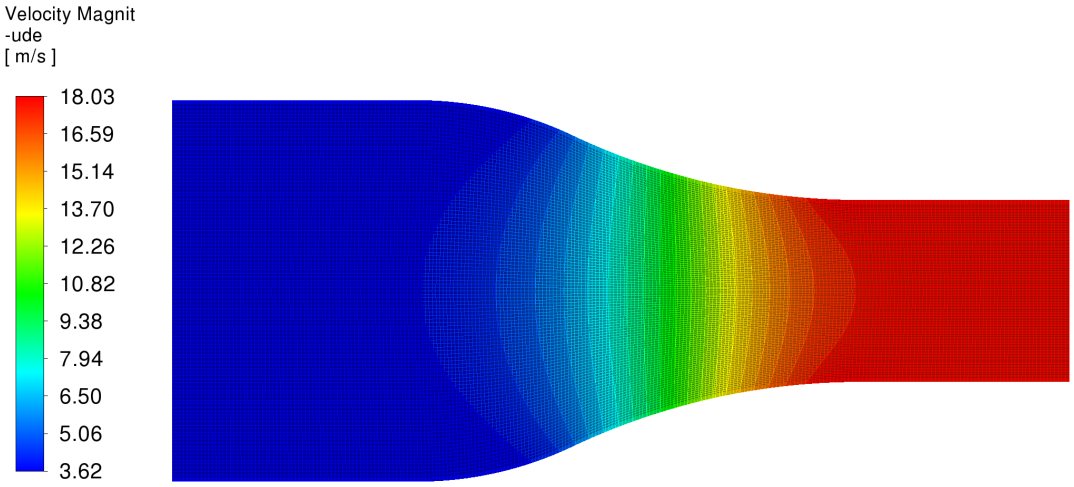

(d) Velocity of hydrogen at 4 m/s

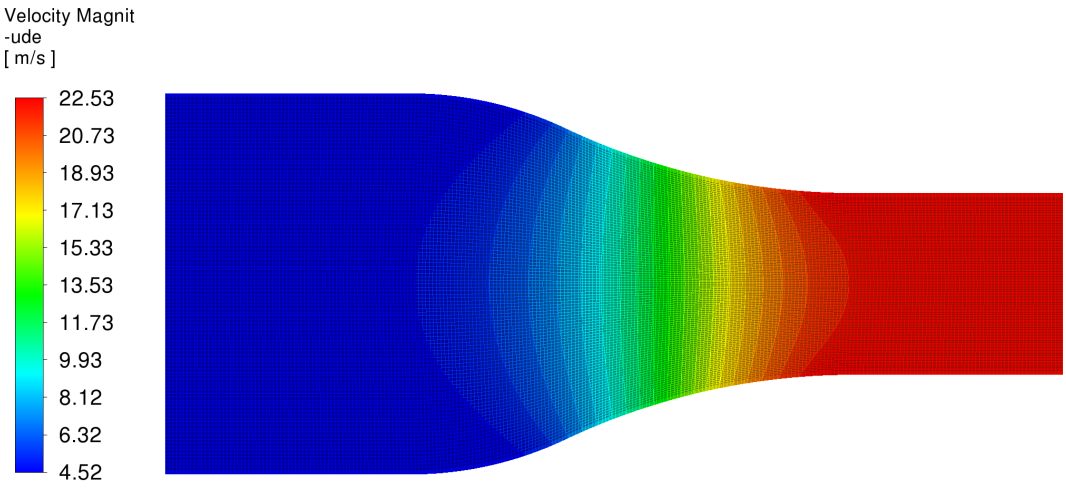

(e) Velocity of hydrogen at 5 m/s

Figure 12. Contour of the velocity of hydrogen

4.2.4 Velocity of hydrogen

Figure 12 shows the data obtained; there is a linear relationship between the hydrogen flow velocity and its velocity magnitude. Each 1 m/s increase in hydrogen flow velocity results in an approximate rise of 4.51 units in velocity magnitude. This indicates that the velocity magnitude is directly proportional to the flow velocity. When the velocity is 1 m/s, the velocity magnitude is 4.51. As the velocity increases to 2 m/s, the magnitude rises to 9.01, showing an increment of 4.50. This pattern continues consistently: for every 1 m/s increase in velocity, the velocity magnitude increases by approximately 4.51 units. At 3 m/s, the velocity magnitude reaches 13.52, while at 4 m/s and 5 m/s, the values are 18.03 and 22.53, respectively.

This linear relationship suggests that fluid density, flow characteristics, or environmental influences are likely constant within the system. In other words, no significant accelerative or resistive forces cause nonlinear changes. This relationship can be mathematically expressed as: Velocity Magnitude = 4.51 × Velocity.

In conclusion, the relationship between hydrogen flow velocity and its velocity magnitude is highly consistent, illustrating a predictable linear pattern. This analysis is critical for practical applications, such as fluid flow simulations or the design of gas transport systems, where an understanding of stable flow dynamics is essential.

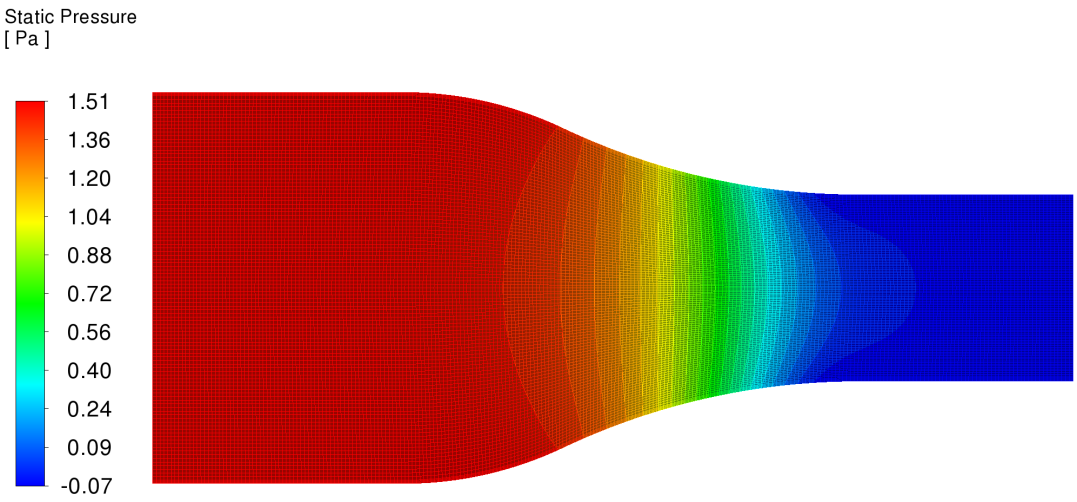

(a) Pressure of helium at 1 m/s

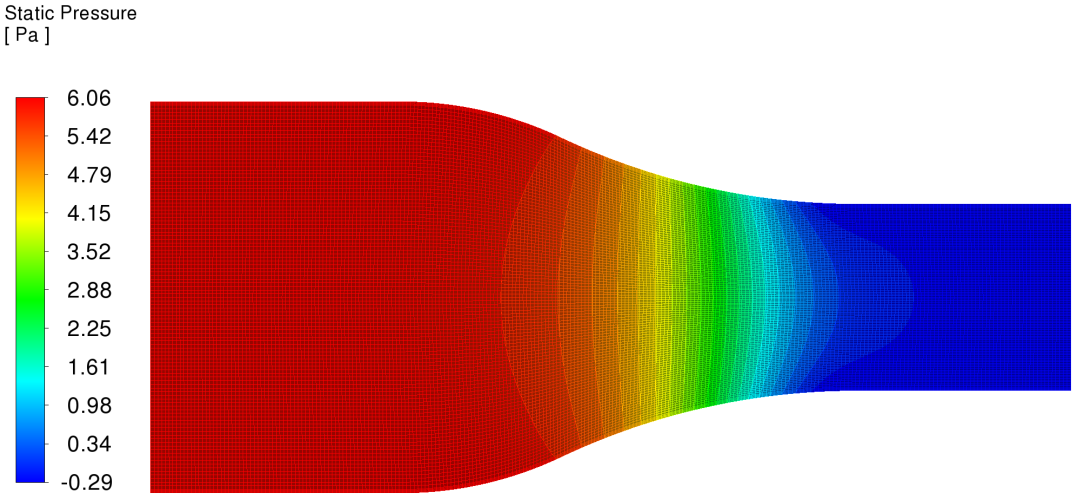

(b) Pressure of helium at 2 m/s

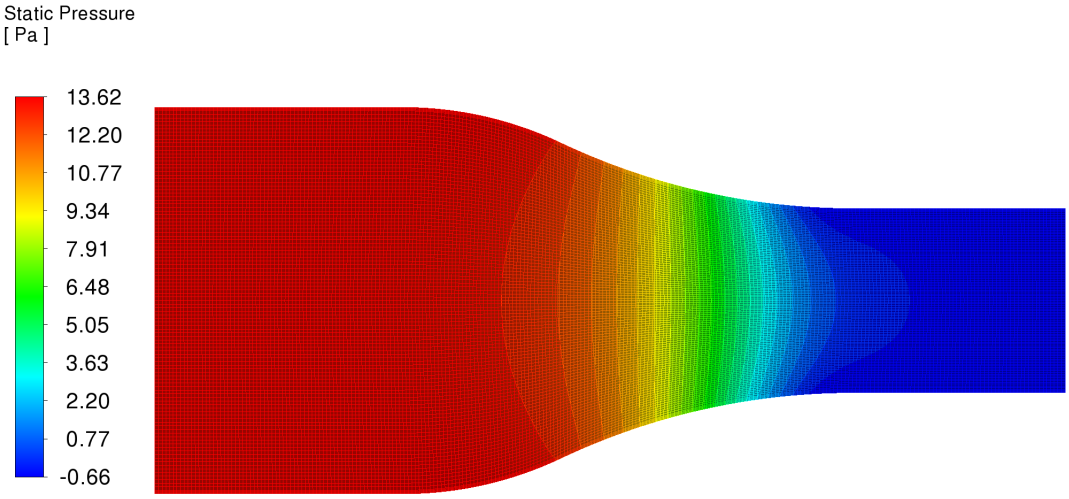

(c) Pressure of helium at 3 m/s

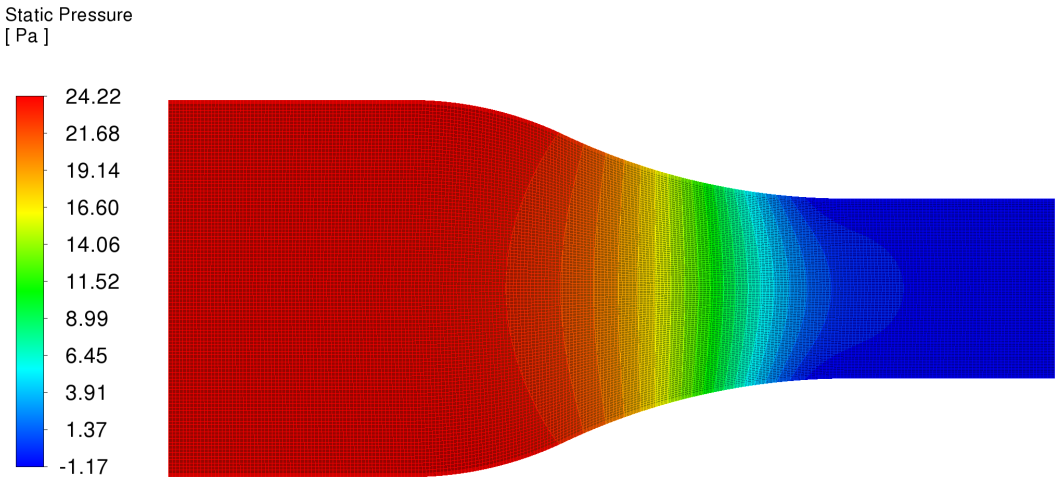

(d) Pressure of helium at 4 m/s

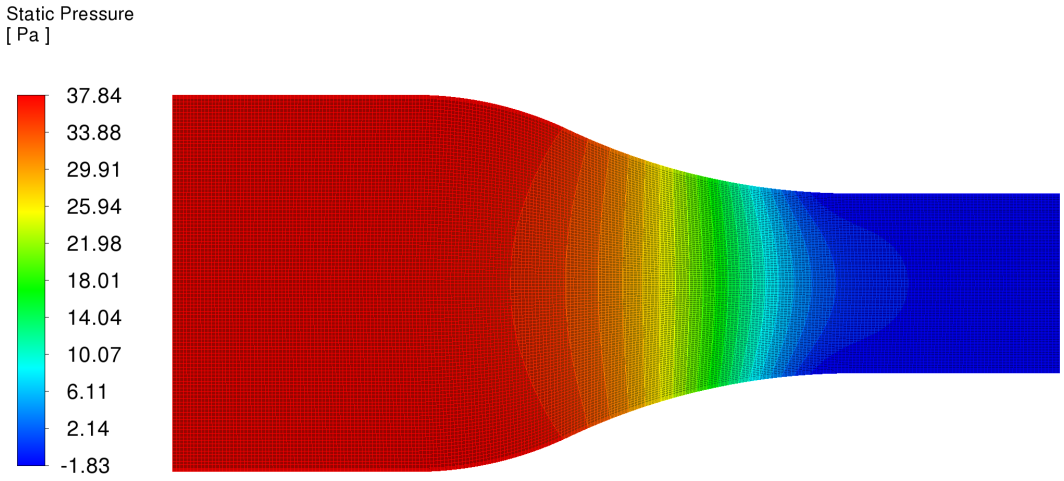

(e) Pressure of helium at 5 m/s

Figure 13. Contour of the pressure of helium

4.2.5 Pressure of helium

Figure 13 illustrates the static pressure distribution of inviscid helium flow through a narrowing channel at varying velocities, ranging from 1 m/s to 5 m/s. The pressure distribution is visualized using a color scale in Pascal (Pa), highlighting variations from maximum pressure in wider channel regions to minimum pressure in the constricted section. This analysis emphasizes the dynamic relationship between flow velocity, channel geometry, and static pressure as described by Bernoulli's principle.

At a velocity of 1 m/s, the maximum pressure is approximately 1.51 Pa, decreasing to -0.07 Pa in the constricted region. With an increase in velocity to 2 m/s, the maximum pressure rises to 6.06 Pa, while the minimum pressure drops to -0.29 Pa. A similar trend is observed at higher velocities: at 3 m/s, the maximum pressure reaches 13.62 Pa, with a minimum of -0.66 Pa; at 4 m/s, the maximum pressure is 24.22 Pa, with a minimum of -1.17 Pa. At the highest velocity analyzed, at 5 m/s, the maximum pressure peaks at 37.84 Pa, and the minimum drops to 1.88 Pa. This trend demonstrates that higher velocities result in more extreme pressure distributions, with maximum and minimum pressures increasing quadratically with velocity.

This pressure distribution reflects the dominant conversion of potential energy to kinetic energy in the inviscid flow system. In wider channel sections, static pressure remains relatively high, indicated by red hues. As the fluid flows into the constricted section, the pressure decreases significantly, transitioning through yellow, green, and blue hues. This phenomenon aligns with Bernoulli's effect, where increased fluid velocity in the narrowing channel causes a corresponding drop in static pressure.

The results of this analysis are critical for fluid system designs, such as nozzles, diffusers, and pipelines, where

precise pressure distribution is essential for improving efficiency and stability. Moreover, the study is relevant for applications in the aeronautical and automotive industries, where understanding ideal fluid dynamics can enhance overall system performance.

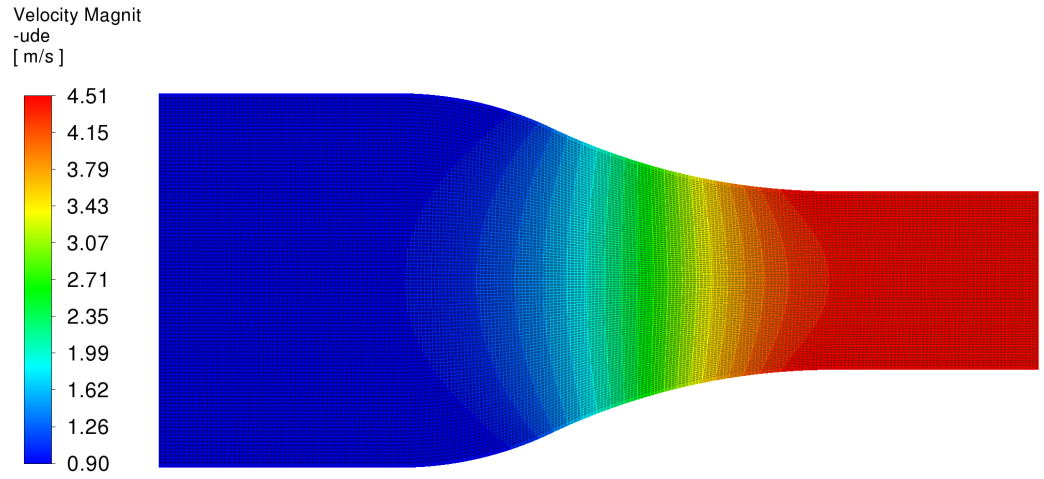

(a) Velocity of helium at 1 m/s

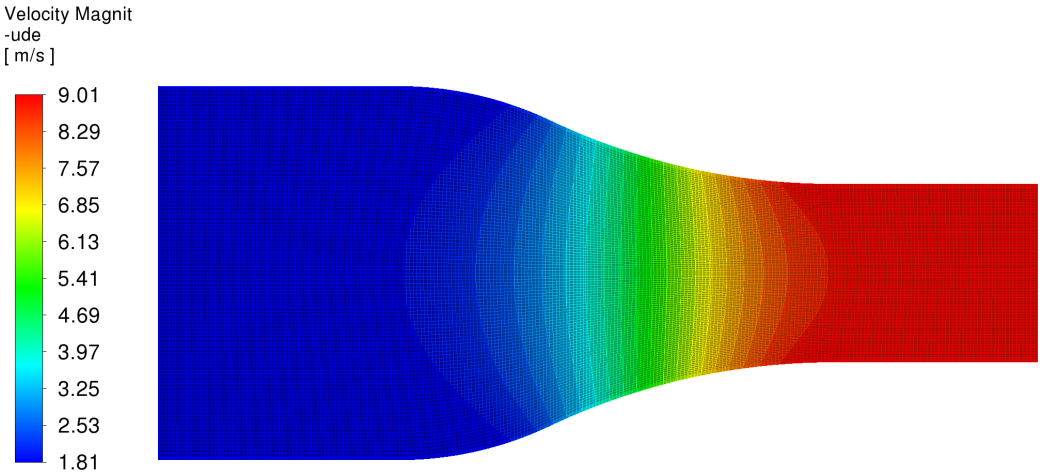

(b) Velocity of helium at 2 m/s

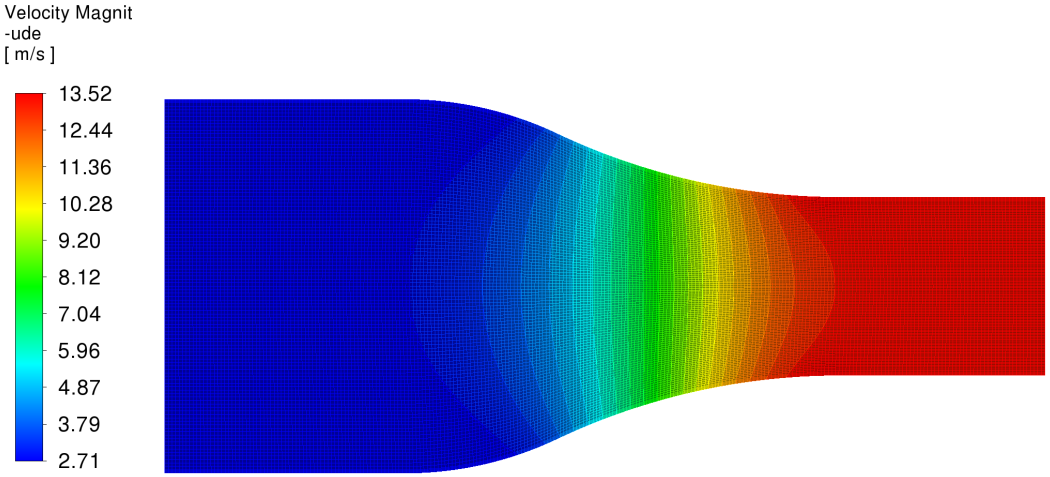

(c) Velocity of helium at 3 m/s

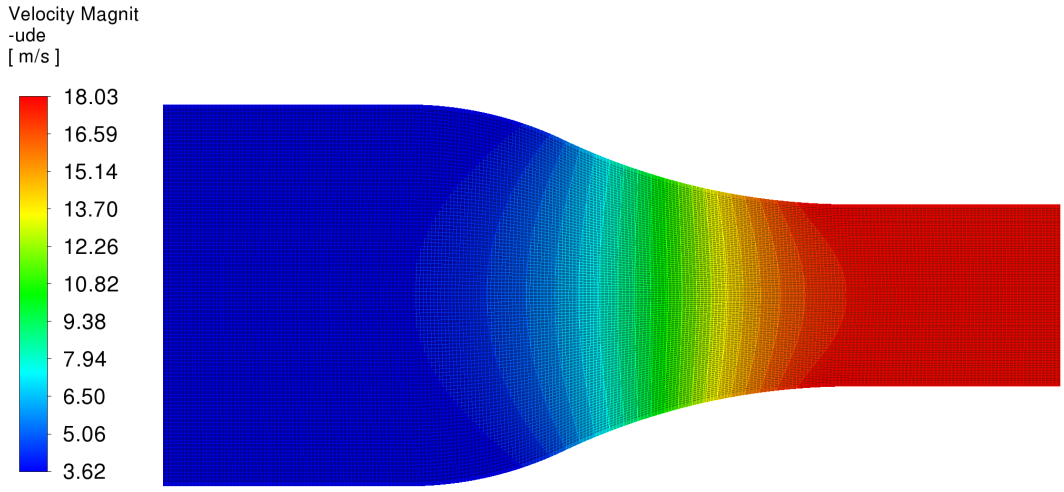

(d) Velocity of helium at 4 m/s

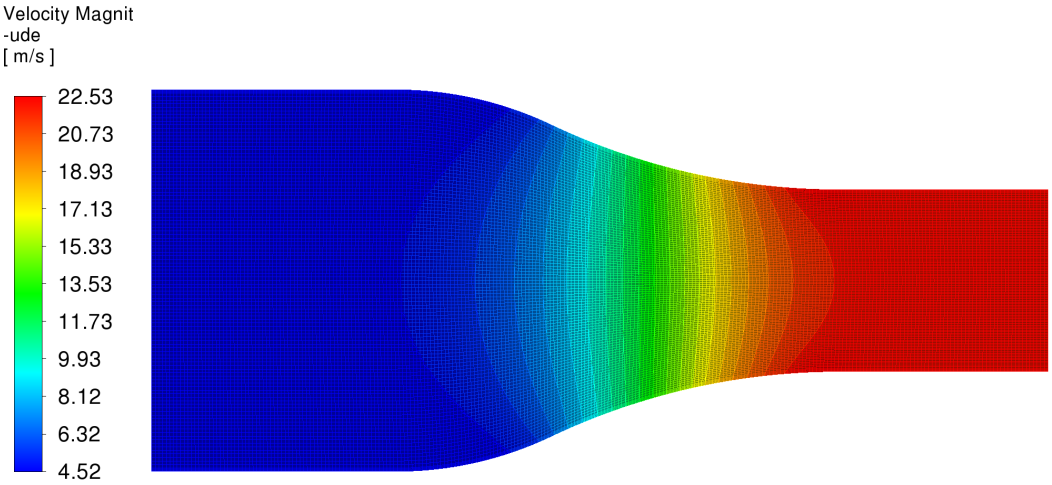

(e) Velocity of helium at 5 m/s

Figure 14. Contour of velocity of helium

4.2.6 Velocity of helium

Figure 14 shows the results of inviscid fluid flow at the nozzle, which show an increase in velocity magnitude proportionally to the inlet velocity range of 1-5 m/s. The highest velocity magnitude values of 4.51, 9.01, 13.52, 18.03, and 22.53 m/s indicate that the fluid experiences significant acceleration when passing through the nozzle. This phenomenon is consistent with Bernoulli's principle, where an increase in fluid velocity in an area with a narrowed cross-sectional area reduces static pressure, increasing fluid kinetic energy. The linear trend in the simulation results reflects idealized conditions without the influence of viscosity, where frictional forces or energy losses do not affect the flow. This pattern shows that ideal inviscid flow in a nozzle result in a maximum velocity distribution that depends directly on the inlet velocity, which is essential in designing high-efficiency flow systems, such as applications in jet engines or other propulsion systems.

The provided figure contains two bar charts comparing static pressure and velocity outlet for viscous and inviscid conditions of three gases: air, helium, and hydrogen. Figure 15 shows static pressure values at five points (P1 to P5) for viscous and inviscid conditions. Air, represented in blue, exhibits significantly higher static pressure values than helium (orange) and hydrogen (gray), especially under inviscid conditions. Figure 16 displays velocity outlet values at five points (V1 to V5) for viscous and inviscid conditions. The velocity outlet values are relatively similar for all three gases, with slight variations between viscous and inviscid conditions. These charts provide a comparative analysis of the behavior of different gases under varying conditions, which is essential for applications in fluid dynamics and engineering, as they highlight how different gases respond to viscous and inviscid environments.

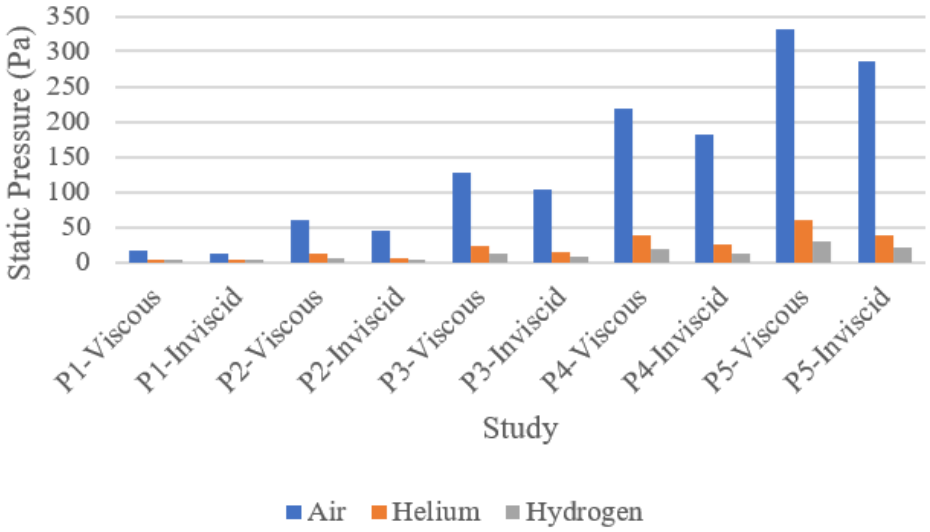

Figure 15. Viscous and inviscid static pressure of air, helium, and hydrogen

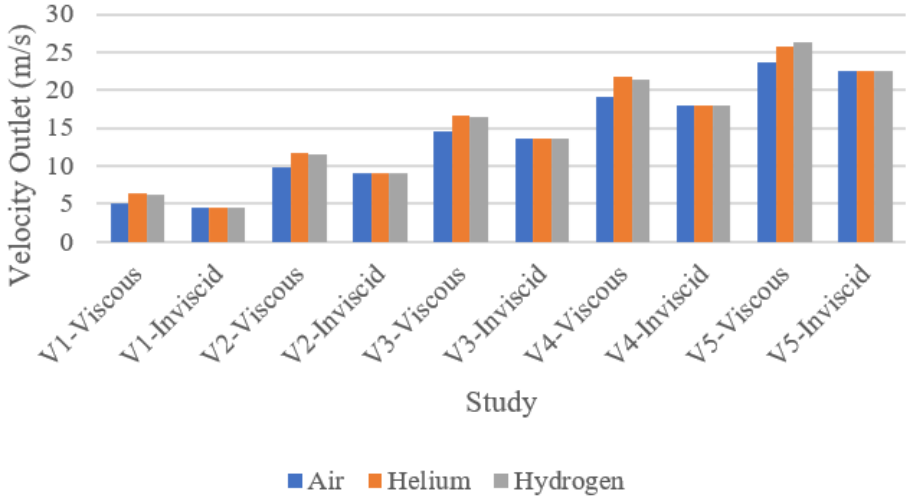

Figure 16. Viscous and inviscid velocity outlet of air, helium, and hydrogen

4.3 Summary of Key Results

The main findings of this study demonstrate that fluid characteristics, such as helium, hydrogen, and air, significantly affect the velocity and static pressure distribution in a convergent-divergent nozzle. With its low density and viscosity, helium exhibits higher velocities and lower pressure drops than hydrogen and air. This highlights helium's efficiency in high-velocity flow applications, such as propulsion and cryogenics. Conversely, with its higher density, air shows more excellent pressure stability, making it ideal for applications requiring precise flow control.

The non-linear relationship between fluid velocity and pressure drop at high velocities becomes increasingly evident. For instance, at an inlet velocity of 5 m/s, helium achieves a maximum velocity of 26.29 m/s, while its static pressure drops significantly to 58.51 Pa. This phenomenon is governed by Bernoulli's principle, where increasing kinetic energy leads to a pressure drop. This analysis underscores the importance of understanding the relationship between velocity and pressure, particularly in nozzle design, to avoid overpressure effects that could damage nozzle structures. However, the individual analysis of fluid characteristics does not fully provide a quantitative comparison. Therefore, the outlet pressure and velocity data were analyzed comparatively. The results indicate that helium has the highest outlet velocity, averaging 22% greater than hydrogen and 35% greater than air. This comparison reinforces the dominance of helium's thermodynamic properties in enhancing flow performance.

The findings of this study are also compared with related literature. For example, Wang et al. [19] noted that fluid viscosity significantly impacts pressure distribution in high-pressure nozzles. This aligns with the findings of this study, which show that low-viscosity fluids like helium result in lower pressure gradients, making them more

efficient in high-flow applications. This difference highlights the importance of selecting the appropriate fluid based on specific application needs.

Furthermore, this discussion identifies the potential non-linear relationship between velocity and pressure at high speeds, which previous studies have not fully explored. This relationship may be linked to the transition from laminar to turbulent flow observed in fluids with high Reynolds numbers. This analysis provides valuable insights for designing nozzles more adaptive to extreme operating conditions.

4.4 ANOVA

In Table 3, the ANOVA results provide a detailed breakdown for the given data set. The total sum of squares for the data is 217,320, with 29 degrees of freedom (DF), resulting in a mean square of 7,493.7. This represents the overall variability in the data set. The model sum of squares, which accounts for the variability explained by the model, is 210,860 with 5 DF, resulting in a mean square of 42,173. This component of the total variability is highly significant, with an F-value of 156.82 and a very low P-value of 1.6379e-17, indicating a strong relationship between the model and the observed data.

Breaking down the model further, the linear component has a sum of squares of 153,930 with 3 DF and a mean square of 51,309. This linear model component shows a significant F-value of 190.8 and a P-value of 7.1317e-17, suggesting a strong linear relationship. The nonlinear component has a sum of squares of 56,935 with 2 DF and a mean square of 28,468, with an F-value of 105.86 and a P-value of 1.2411e-12, indicating that the nonlinear relationships also contribute significantly to the model.

The residual sum of squares, representing the unexplained variability or error, is 6,454.1 with 24 DF, leading to a mean square of 268.92. This residual component helps assess the model's goodness of fit. Within the residual, the lack of fit has a sum of squares of 3,911.7 with 9 DF and a mean square of 434.63. The F-value for lack of fit is 2.5643, with a P-value of 0.051591, just above the typical significance level of 0.05, suggesting that the lack of fit may not be highly significant. Finally, the pure error, the variability due to random error, has a sum of squares of 2,542.4 with 15 DF and a mean square of 169.49. In summary, Table 3 indicates that the model's linear and nonlinear components are highly significant, explaining a substantial portion of the variability in the data. The residual error is relatively low, and while the lack of fit is not highly important, it suggests that the model fits the data reasonably well.

Table 3. ANOVA

Properties	SumSq	DF	MeanSq	F	P-value
Total	$2.1732e+05$	29	7493.7		
Model	$2.1086e+05$	5	42173	156.82	1.6379e-17
- Linear	$1.5393e+05$	3	51309	190.8	7.1317e-17
- Nonlinear	56935	2	28468	105.86	1.2411e-12
Residual	6454.1	24	268.92		
- Lack of fit	3911.7	9	434.63	2.5643	0.051591
- Pure error	2542.4	15	169.49		

4.5 Future Applications and Research Directions

4.5.1 Future applications

The insights from this study have several potential applications in various engineering fields where fluid flow plays a critical role. By integrating soft computing and data mining techniques, these applications can be further enhanced:

• **Aerospace propulsion:** The study's findings on low-density gases like hydrogen and helium can inform the design of lightweight and high-efficiency propulsion systems. Soft computing methods like genetic algorithms can optimize nozzle geometries to achieve optimal thrust and minimize fuel consumption.

• **Cryogenics and energy systems:** In cryogenic systems, where helium is commonly used, understanding flow dynamics can improve the efficiency of cooling processes. Data mining techniques can be applied to analyze historical system performance data, identify anomalies, and optimize operational conditions to enhance system reliability.

• **Gas transport and storage:** Hydrogen transport in pipelines is critical for transitioning to green energy. The findings can support pipeline design to reduce pressure drops and energy losses. Based on operational data, machine learning models can predict failure risks or leaks, enhancing safety and efficiency.

• **Chemical processing:** Using nitrogen and other gases in industrial processes can benefit from the study's insights. Fuzzy logic systems can be integrated into real-time process control, allowing adjustments based on fluid properties and flow conditions to maintain optimal processing parameters.

4.5.2 Suggestion for future research

• **Integration of soft computing models:** Future studies could integrate ANNs or fuzzy inference systems to predict flow patterns under diverse operating conditions. These models can complement CFD simulations by providing faster approximations of flow behavior.

• **Data-driven pattern recognition:** Incorporating data mining techniques, such as clustering or principal component analysis, could help identify hidden patterns or anomalies in simulation results. This approach can uncover subtle dependencies between fluid properties, boundary conditions, and flow outcomes.

• **Hybrid simulation frameworks:** Combining CFD models with soft computing approaches, such as neuro-fuzzy systems, could enhance accuracy in predicting complex flow behaviors. This hybrid methodology would be beneficial for turbulence or non-linear interaction scenarios.

• **Optimization studies:** Future research could apply optimization algorithms, such as PSO or simulated annealing, to refine nozzle designs or boundary conditions for improved flow efficiency and reduced energy consumption.

• **Expansion to multi-phase flows:** Extending the study to multi-phase flows involving gases and liquids could provide insights into more complex systems. Machine learning models could assist in characterizing interactions between phases, improving the predictive capabilities of simulations. By leveraging the potential of soft computing and data mining, future researchers can expand the scope of this work, providing more efficient solutions and deeper insights into fluid dynamics.

5 Conclusions

In the analysis of viscous and inviscid fluids for water, helium, and hydrogen with velocities between 1 and 5 m/s, Bernoulli's theorem shows that an increase in velocity in an inviscid fluid leads to a decrease in static pressure, with helium reaching a top velocity of 25. In contrast, analysis using the Navier-Stokes equations for viscous liquids such as water shows that viscosity affects the velocity distribution in laminar flow, where the outlet velocity of water increases from 5.13 m/s to 23.63 m/s at different viscous conditions. A comparison between these three types of fluids shows that helium has the most efficient flow rate, followed by hydrogen and water. Understanding viscosity and density properties is essential in designing fluid flow systems. Bernoulli's theorem and the Navier-Stokes equations help predict and optimize system performance for various industrial applications, from aerodynamics to piping engineering. Further experimental validation and testing are required to refine the theoretical models used.

Simulation analysis of fluid mechanics at the nozzle using air, hydrogen, and helium shows different behavior based on the physical properties of each fluid. Air, with its higher density and lower kinematic viscosity, exhibits relatively stable flow characteristics and is closer to the inviscid assumption, especially at low to medium speeds. In contrast, hydrogen and helium, which have lower densities but relatively more dominant viscosities, show higher sensitivity to the influence of frictional forces, especially in narrow geometries such as nozzles. In the inviscid flow scenario, the flow pattern is entirely determined by the variation of pressure and velocity according to Bernoulli's principle, resulting in almost uniform behavior for all three fluids. However, when viscosity effects are considered, hydrogen and helium show sharper differences in pressure and velocity distributions than air, reflecting the strong influence of viscous forces. These findings emphasize the importance of considering viscosity effects in nozzle design, especially for low-density fluids such as hydrogen and helium. Meanwhile, the inviscid assumption often remains an adequate approach for air fluids and provides accurate predictive results with more straightforward calculations.

This analysis shows that selecting the fluid type and understanding viscosity properties are critical in designing fluid flow systems. Specific recommendations include optimizing nozzle geometry to account for the viscosity effects of hydrogen and helium, particularly in narrow geometries, to minimize frictional losses and improve flow efficiency. Gas selection should also consider density and viscosity properties to match application requirements, such as prioritizing helium for high-efficiency flow systems or air for scenarios where inviscid assumptions suffice. Bernoulli's theorem and the Navier-Stokes equations provide robust tools for predicting and optimizing system performance across various industrial applications, including aerodynamics, piping engineering, and nozzle design. Further experimental validation and testing are required to refine the theoretical models and validate these design recommendations.

Data Availability

The data used to support the findings of this study are available from the corresponding author upon request.

Conflicts of Interest

The authors declare no conflict of interest.

References

[1] N. Pourmahmoud, M. Rashidzadeh, and A. Hassanzadeh, "CFD investigation of inlet pressure effects on the energy separation in a vortex tube with convergent nozzles," *Eng. Comput.*, vol. 32, no. 5, pp. 1323–1342, 2015. https://doi.org/10.1108/EC-06-2014-0125

[2] K. M. Pandey and A. P. Singh, "CFD analysis of conical nozzle for mach 3 at various angles of divergence with fluent software," *Int. J. Chem. Eng. Appl.*, vol. 1, no. 2, pp. 179–185, 2010. https://doi.org/10.7763/IJCEA.2010.V1.31

[3] M. Kumar, R. K. Sahoo, and S. K. Behera, "Design and numerical investigation to visualize the fluid flow and thermal characteristics of non-axisymmetric convergent nozzle," *Eng. Sci. Technol. Int. J.*, vol. 22, no. 1, pp. 294–312, 2019. https://doi.org/10.1016/j.jestch.2018.10.006

[4] M. Khan, M. Zunaid, and Q. Murtaza, "Computational simulation of cold spray coating for optimal injector length," *Case Stud. Therm. Eng.*, vol. 51, p. 103655, 2023. https://doi.org/10.1016/j.csite.2023.103655

[5] Z. Arifin, S. D. Prasetyo, B. A. Tribhuwana, D. D. D. P. Tjahjana, R. A. Rachmanto, and B. Kristiawan, "Photovoltaic performance improvement with phase change material cooling treatment," *Int. J. Heat Technol.*, vol. 40, no. 4, pp. 953–960, 2022. https://doi.org/10.18280/ijht.400412

[6] H. D. Kim, J. H. Lee, K. A. Park, T. Setoguchi, and S. Matsuo, "A study of the critical nozzle for flow rate measurement of high-pressure hydrogen gas," *J. Therm. Sci.*, vol. 16, no. 1, pp. 28–32, 2007. https://doi.org/10.1007/s11630-007-0028-z

[7] J. Kumari and C. S. Koli, "Modelling and simulation of supersonic nozzle using ANSYS workbench with new measuring data," *Int. J. Sci. Res. Dev.*, vol. 4, no. 11, pp. 553–556, 2017.

[8] Z. Arifin, D. D. D. P. Tjahjana, R. A. Rachmanto, S. Suyitno, S. D. Prasetyo, and T. Trismawati, "Redesign mata bor tanah untuk pembuatan lubang biopori di desa Puron, kecamatan Bulu, kabupaten Sukoharjo," *Mek. Maj. Ilm. Mek.*, vol. 19, no. 2, pp. 60–67, 2020. https://doi.org/10.20961/mekanika.v19i2.43393

[9] B. Debtera, V. Sundramurthy, and N. Ibsa, "Computational fluid dynamics simulation and analysis of fluid flow in pipe: Effect of fluid viscosity," *J. Comput. Theor. Nanoscience*, vol. 18, no. 3, pp. 805–810, 2021. https://doi.org/10.1166/jctn.2021.9680

[10] A. Y. W. Chong, K. W. Khaw, W. C. Yeong, and W. X. Chuah, "Customer churn prediction of telecom company using machine learning algorithms," *J. Soft Comput. Data Min.*, vol. 4, no. 2, pp. 1–22, 2023. https://doi.org/10.30880/jscdm.2023.04.02.001

[11] Y. Trisnoaji, S. D. Prasetyo, M. S. Mauludin, C. Harsito, and A. Anggit, "Computational fluid dynamics evaluation of nitrogen and hydrogen for enhanced air conditioning efficiency," *J. Ind. Intell.*, vol. 2, no. 3, pp. 144–159, 2024. https://doi.org/10.56578/jii020302

[12] S. D. Prasetyo, Z. Arifin, A. R. Prabowo, and E. P. Budiana, "Investigation of the addition of fins in the collector of water/Al2O3-based PV/T system: Validation of 3D CFD with experimental study," *Case Stud. Therm. Eng.*, vol. 60, p. 104682, 2024. https://doi.org/10.1016/j.csite.2024.104682

[13] A. Khan, A. Aabid, and S. A. Khan, "CFD analysis of convergent-divergent nozzle flow and base pressure control using micro-JETS," *Int. J. Eng. Technol.*, vol. 7, no. 3, pp. 232–235, 2018. https://doi.org/10.14419/ijet.v7i3.29.18802

[14] R. A. Mugher and N. A. M. Alhammadi, "Performance evaluation of quadratic probing and random probing algorithms in modeling hashing technique," *J. Soft Comput. Data Min.*, vol. 3, no. 2, pp. 52–59, 2022. https://doi.org/10.30880/jscdm.2022.03.02.006

[15] G. S. Narayan, V. Chobey, P. M. Kiran, and M. Baranwal, "A research paper on analysis of de-Laval nozzle on ansys workbench," *Int. Res. J. Eng. Technol.*, vol. 6, no. 11, pp. 471–477, 2019.

[16] P. Adibi, R. Bagheri, and M. Hosseini, "Numerical simulation of cavitating flow in liquid nitrogen through a convergent nozzle," *Heliyon*, vol. 10, no. 16, p. e36359, 2024. https://doi.org/10.1016/j.heliyon.2024.e36359

[17] A. S. Sha'ari and Z. Abdullah, "A comparative study between machine learning and deep learning algorithm for network intrusion detection," *J. Soft Comput. Data Min.*, vol. 3, no. 2, pp. 43–51, 2022. https://doi.org/10.30880/jscdm.2022.03.02.005

[18] A. H. Abdulkarim, E. Canli, and A. Ateş, "CFD case study on a nozzle flow literature review, theoretical framework, tools and educational aspects," in *International Conference on Engineering Technologies*, Konya, Turkey, 2018, pp. 486–489.

[19] D. Wang, Y. Gu, C. Stephen, W. Zhao, and Q. Ji, "Assessment of viscosity effects on high-speed coolant pump performance," *Phys. Fluids*, vol. 36, p. 055107, 2024. https://doi.org/10.1063/5.0208753

[20] N. L. Rakesh and K. Rambalaji, "Analysis of flow of nozzles by using computational fluid dynamics," *Int. J. Psychosoc.*, vol. 23, no. 3, pp. 390–399, 2019. https://doi.org/10.37200/IJPR/V23I3/PR190137

[21] S. Huang, Y. L. Zhang, X. X. Yin, M. X. Zhang, and et al., "Effect of nozzle quantity on the flow field characteristics

and grinding efficiency in a Steam Jet Mill," *Processes*, vol. 12, no. 7, 2024. https://doi.org/10.3390/pr12071500

[22] Y. Trisnoaji, S. D. Prasetyo, C. Harsito, A. Anggit, and M. Subchan, "Exploring pressure dynamics in rough-surfaced U-Bend pipelines: A comparative study of water and nanofluid composites across varying mass flow rates," *Sem. Int. J. Nanotechnol.*, vol. 3, no. 1, pp. 1–21, 2024.

[23] K. Kovacic, S. Bajt, and B. Šarler, "Numerical analysis of Knudsen number of helium flow through gas-focused liquid sheet micro-nozzle," *Fluids*, vol. 9, no. 12, p. 273, 2024. https://doi.org/10.3390/fluids9120273

[24] D. F. Hanan, G. M. Lazuardi, Y. Trisnoaji, S. D. Prasetyo, and et al., "Thermal and hydrodynamic performance analysis of water-cooled heat sinks using aluminum and structural steel materials," *Power Eng. Eng. Thermophys.*, vol. 3, no. 3, pp. 176–188, 2024. https://doi.org/10.56578/peet030303

[25] D. Erwanto, R. F. Rizal, D. E. Yuliana, M. Munir, Y. Trisnoaji, C. Harsito, A. A. Mahadi, and S. D. Prasetyo, "Development and application of an electronic nose system based on ARM9," *Nongye Jixie Xuebao*, vol. 40, no. 1, pp. 138–142, 2009.

[26] J. M. R. Gorle, B. F. Terjesen, and S. T. Summerfelt, "Hydrodynamics of Atlantic salmon culture tank: Effect of inlet nozzle angle on the velocity field," *Comput. Electron. Agric.*, vol. 158, pp. 79–91, 2019. https://doi.org/10.1016/j.compag.2019.01.046

[27] G. K. Costa, P. R. M. Lyra, and C. A. B. D. O. Lira, "Numerical simulation of two dimensional compressible and incompressible flows," *J. Braz. Soc. Mech. Sci. Eng.*, vol. 27, no. 4, pp. 372–380, 2005. https://doi.org/10.1590/S1678-58782005000400005

[28] D. Barale, G. Limbardi, and R. R. Arakerimath, "Modelling and parametric fluid flow analysis (CFD) and effect on convergent nozzle used in Pelton turbine," *J. Emerg. Technol. Innov. Res.*, 2016.

[29] P. Jayaprakash, D. Dhinarakaran, and D. Das, "Design and analysis of a rocket C-D nozzle," *Int. J. Health Sci. (Qassim)*, vol. 6, no. S5, pp. 3545–3559, 2022. https://doi.org/10.53730/ijhs.v6ns5.9404

[30] K. Bittner, N. Margaritis, F. Schulze-küppers, J. Wolters, and G. Natour, "Computational fluid dynamics modelling of hydrogen production via water splitting in oxygen membrane reactors," *Membranes*, vol. 14, no. 10, p. 219, 2024. https://doi.org/10.3390/membranes14100219

[31] K. Yassin, S. Kelm, M. Kampili, and E. A. Reinecke, "Validation and verification of containmentFOAM CFD simulations in hydrogen safety," *Energies*, vol. 16, no. 16, p. 5993, 2023. https://doi.org/10.3390/en16165993

[32] M. Li, S. Q. Chen, W. D. Jiang, Y. C. Li, and et al., "Numerical simulation analysis of the hydrogen-blended natural gas leakage and ventilation processes in a domestic house," *ACS Omega*, vol. 8, no. 38, pp. 34 610–34 628, 2023. https://doi.org/10.1021/acsomega.3c03551

[33] K. Nirmaladevi, M. Mythilee, M. Navein, and K. Manikandaprabhu, "A study on Bernoulli's equation & its application in fluid mechanics," *Int. J. Sci. Res. Dev.*, vol. 6, no. 12, pp. 223–225, 2019.

[34] J. P. Thavamani, "Bernoulli equation in fluid flow," *Int. J. Curr. Res.*, vol. 8, no. 10, pp. 40 459–40 461, 2016.

[35] M. L. Kavvas and A. Ercan, "Generalizations of incompressible and compressible Navier–Stokes equations to fractional time and multi-fractional space," *Sci. Rep.*, vol. 12, p. 19337, 2022. https://doi.org/10.1038/s41598-022-20911-3

[36] S. Sklarz and L. P. Horwitz, "Relativistic mechanics of continuous media," *Found. Phys.*, vol. 31, pp. 909–934, 2001. https://doi.org/10.1023/A:1017559901338

[37] T. M. Adams and A. Raghunandan, "Modified bernoulli equation for use with combined electro-osmotic and pressure-driven microflows," in *Proceeding of Proceedings of the 23rd CANCAM*, 2012.

[38] S. V. Ershkov and R. V. Shamin, "A riccati-type solution of 3D Euler equations for incompressible flow," *J. King Saud Univ. Sci.*, vol. 32, no. 1, pp. 125–130, 2020. https://doi.org/10.1016/j.jksus.2018.03.010